UNIVERSIDADE DE SÃO PAULO

Instituto de Ciências Matemáticas e de Computação

A Numerical Method for Solving Three-Dimensional Generalized Newtonian Free Surface Flows

M.F. Tomé
L. Grossi
A.Castelo
J.A. Cuminato
N. Mangiavacchi
V.G. Ferreira
F.S. de Sousa
S. McKee

Nº 71

NOTAS

São Carlos - SP

UNIVERSIDADE DE SÃO PAULO
Instituto de Ciências Matemáticas e de Computação
ISSN 0103-2577

A Numerical Method for Solving Three-Dimensional Generalized Newtonian Free Surface Flows

M.F. Tomé
L. Grossi
A.Castelo
J.A. Cuminato
N. Mangiavacchi
V.G. Ferreira
F.S. de Sousa
S. McKee

Nº 71

NOTAS

Série Computação

São Carlos – SP
Jul./2003

Resumo

Esse trabalho apresenta um método numérico para resolver escoamentos tridimensionais com superfícies livres de um fluido generalizado. O método numérico desenvolvido nesse trabalho é uma extensão da técnica de diferenças finitas introduzida por Tomé, McKee e Duffy para três dimensões e adicionalmente inclui muitos outros melhoramentos. As equações governantes são resolvidas pelo método de diferenças finitas numa malha diferenciada. O fluido é representado por particulas marcadoras que fornecem a localização e visualização da superfície livre do fluido. Como implementado, este método numérico pode ser aplicado para simular escoamentos de fluidos generalizados governados pelo modelo de Cross. A técnica numérica apresentada nesse trabalho foi validada comparando-se os resultados numéricos com soluções analíticas obtidas do escoamento de um fluido definido pelo modelo de Cross dentro de um tubo. São também apresentados resultados numéricos do escoamento de um jato de fluido generalizado escoando sobre uma superfície planar e a simulação de 'jet buckling'.

A Numerical Method for Solving Three-Dimensional Generalized Newtonian Free Surface Flows

M.F. Tomé, L. Grossi,
A. Castelo,
J.A. Cuminato,
N. Mangiavacchi,
V. G. Ferreira,
F. S. de Sousa

Universidade de São Paulo
Instituto de Ciências Matemáticas e de Computação
Departamento de Ciências de Computação e Estatística
Avenida Trabalhador Sãocarlense, 400 - Caixa Postal 668
São Carlos - SP - Brasil
CEP 13560-970

S. McKee[1]

University of Strathclyde
Department of Mathematics
26 Richmond Street
Glasgow - UK - G1 1XH

Abstract

This work presents a numerical technique for solving three-dimensional generalized Newtonian free surface flows. It is an extension to three dimensions of the technique introduced by Tomé, McKee and Duffy [18] but additionally includes many other features. The governing equations are solved by a finite difference method on a staggered grid. It uses marker particles to describe the fluid; these particles provide the location and visualization of the fluid free surface. As currently implemented, the present method can simulate generalized Newtonian flow in which the viscosity is modelled using the Cross model. The numerical technique presented in this paper is validated by using exact solutions for the flow of a Cross model fluid inside a pipe. Numerical results showing the flow of a generalized Newtonian fluid jet impinging onto a flat surface and that of a jet buckling are given.

[1]Corresponding Author

1. Introduction

Non-Newtonian fluid flows with free surfaces appear in many technological processes: container filling, injection moulding, ink-jet printers and wire coating. The main motivation for this work has come from the food and domestic products industries where the materials tend to be shear-thinning.

The rheology community has been extremely active in developing numerical methods over the last twenty years. For the most part effort has focussed on solving the upper convected Maxwell (UCM) model and the Oldroyd-B model (see, eg. [4]). The integral equivalent of the UCM model has also found favour (see, eg. [3]). The game has been to crack the "High Weissenberg Number Problem" and the principal players have included Crochet and his team at Leuven, Armstrong and Brown at MIT and Tanner and Phan-Thien at Sydney; a recent interesting book by Tanner and Walters [17] provides a comprehensive history of the state of rheology today and a daunting number of references. Despite this effort little has been done in three dimensions, although the recent papers by Xue et al. ([25], [26]) are worth noting. Free surface flows are also an area that does not appear to have received a great deal of attention. Exceptions include the work of Sato and Richardson [15] who incorporate marker and cell ideas with a finite element code for viscoelastic fluids, and the finite element injection moulding of Manogg et al. [13] where the viscosity is modelled by Yasuda-Carreau viscosity model which depends upon both the temperature and the rate of strain tensor. However, possibly the principal exception is the work by Luo [11] who studies the now classical rod-climbing phenomenon. The work is performed in two dimensions (axisymmetric flow) and, although the results are impressive, one has to wonder whether the time evolution of the flow is truly axisymmetric.

This paper is a considerable extension of an earlier two-dimensional generalised Newtonian flow (Tomé et al. [18]). It is concerned with the full three-dimensional shear-thinning, multiple free surface flows and is based on a generalised Newtonian fluid with the viscosity related to the shear rate by the Cross model, or some similar model. It originated from the ideas of the marker-and-cell (MAC) methodology with particular focus on the SMAC (Simplified MAC) method (Amsden and Harlow [1]). The MAC method was of course first introduced by Harlow and Welch [10] at the Los Alamos Scientific Laboratory in the early 1960s. However, many hundreds of papers have bveen published on this technique over the last four decades; recent books by Shyy et al. [16] and Griebel et al. [9] provide excellent overviews.

The present paper solves for the flow and pressure fields of a transient non-Newtonian fluid on a highly irregular three-dimensional region with multiple free surfaces, and with the viscosity depending in a prescribed way upon the local shear rate. The key features of the method proposed are the accurate approximation of the free surface boundary conditions, the adaptive time-stepping routine and the ability to only retain particles (markers) near to the surface or surfaces by deletion and insertion. High order bounded upwinding schemes permit calculations with high Reynolds numbers (up to 2000). The code is embedded within a solid modelling shell which permits output in the form of three-dimensional colour pictures with all the usual solid modelling attributes (for details, see Castelo et al. [2]). The purpose of the paper is to describe the numerical algorithm in just sufficient detail to make it reproducible and, at the same time, display the results of the application of the code to three problems: jet impingement, jet buckling and drop spreading. In addition, pipe flow and Couette flow are used to validate

the code.

2. Governing Equations

The basic equations for the flow of an incompressible generalized fluid with density ρ can be written as

$$\rho\frac{D\mathbf{u}}{Dt} = \nabla\cdot\underline{\underline{\sigma}} + \rho\mathbf{g}\ , \quad \nabla\cdot\mathbf{u} = 0 \tag{1}$$

where $\mathbf{u}(\mathbf{x},t)$, $\underline{\underline{\sigma}}(\mathbf{x},t)$ and $\mathbf{g}$ denote the fluid velocity, the stress tensor and the gravitational acceleration, respectively. The stress tensor is required to obey the constitutive equations

$$\underline{\underline{\sigma}} = -p\underline{\underline{\mathbf{I}}} + 2\mu(q)\,\underline{\underline{\mathbf{d}}} \tag{2}$$

where p is the fluid pressure, $\underline{\underline{\mathbf{I}}}$ is the identity tensor, $\underline{\underline{\mathbf{d}}}$ is the rate-of-deformation tensor given by

$$\underline{\underline{\mathbf{d}}} = \frac{1}{2}\left[(\nabla\mathbf{u}) + (\nabla\mathbf{u})^T\right]\ , \tag{3}$$

q is the local shear rate defined by

$$q = \left[2\mathrm{tr}(\underline{\underline{\mathbf{d}}}^2)\right]^{1/2}\ , \tag{4}$$

and $\mu(q)$ is the apparent viscosity (a prescribed function of q). Introducing (2) and (3) into (1) we obtain

$$\frac{D\mathbf{u}}{Dt} = -\nabla p + \nu(q)\nabla^2\mathbf{u} + \nabla\nu(q)\left[(\nabla\mathbf{u}) + (\nabla\mathbf{u})^{\mathrm{T}}\right] + \mathbf{g}\ , \tag{5}$$

$$\nabla\cdot\mathbf{u} = 0\ , \tag{6}$$

where $\nu(q)$ is the kinematic viscosity.

We shall consider unsteady free-surface flows of a viscous fluid moving into a passive atmosphere (which we may take to be at zero pressure). In the absence of surface tension the normal and tangential components of stress must be continuous across any free surface, so that on such a surface

$$\mathbf{n}\cdot(\underline{\underline{\sigma}}\cdot\mathbf{n}) = 0 \quad \text{and} \quad \mathbf{m}\cdot(\underline{\underline{\sigma}}\cdot\mathbf{n}) = 0, \tag{7}$$

where $\mathbf{n}$ and $\mathbf{m}$ denote unit normal and tangent vectors to the surface and $\underline{\underline{\sigma}}$ denotes the stress tensor.

We also have the no-slip condition ($\mathbf{u} = \mathbf{0}$) on fixed boundaries. Other boundary conditions, such as those at an entry or exit port of the (computational) domain, are discussed in Tomé et al. [18].

We consider three-dimensional flows and use Cartesian coordinates, with $\mathbf{u} = (u(x,y,z,t), v(x,y,z,t), w(x,y,z,t))$ and $p = p(x,y,z,t)$. Let L, U and ν_0 denote 'typical' length, velocity and viscosity scales and introduce the nondimensionalization

$$\mathbf{u} = U\bar{\mathbf{u}}, \quad \mathbf{x} = L\bar{\mathbf{x}}, \quad \nu = \nu_0\bar{\nu}, \quad q = \frac{U}{L}\bar{q}, \quad t = \frac{L}{U}\bar{t}, \quad p = \rho U^2\bar{p}, \quad \mathbf{g} = g\bar{\mathbf{g}},$$

where $g = |\mathbf{g}|$ (so that $\bar{\mathbf{g}}$ is a unit vector). For the sake of clarity we drop the overbars so that equations (5) and (6) may be written as

$$\frac{\partial \mathbf{u}}{\partial t} = -\nabla p + N(\mathbf{u}) \tag{8}$$

$$\frac{\partial u}{\partial x} + \frac{\partial v}{\partial y} + \frac{\partial w}{\partial z} = 0 \tag{9}$$

where $N(\mathbf{u})$ has components

$$\begin{aligned} N_1 = & -\frac{\partial u^2}{\partial x} - \frac{\partial (uv)}{\partial y} - \frac{\partial (uw)}{\partial z} + \frac{1}{Re}\nu(q)\left[\frac{\partial^2 u}{\partial x^2} + \frac{\partial^2 u}{\partial y^2} + \frac{\partial^2 u}{\partial z^2}\right] \\ & + \frac{1}{Re}\left[2\frac{\partial u}{\partial x}\frac{\partial \nu}{\partial x} + \left(\frac{\partial u}{\partial y} + \frac{\partial v}{\partial x}\right)\frac{\partial \nu}{\partial y} + \left(\frac{\partial u}{\partial z} + \frac{\partial w}{\partial x}\right)\frac{\partial \nu}{\partial z}\right] + (1/Fr^2)g_x \end{aligned} \tag{10}$$

$$\begin{aligned} N_2 = & -\frac{\partial (uv)}{\partial x} - \frac{\partial (v^2)}{\partial y} - \frac{\partial (vw)}{\partial z} + \frac{1}{Re}\nu(q)\left[\frac{\partial^2 v}{\partial x^2} + \frac{\partial^2 v}{\partial y^2} + \frac{\partial^2 v}{\partial z^2}\right] \\ & + \frac{1}{Re}\left[\left(\frac{\partial u}{\partial y} + \frac{\partial v}{\partial x}\right)\frac{\partial \nu}{\partial x} + 2\frac{\partial v}{\partial y}\frac{\partial \nu}{\partial y} + \left(\frac{\partial v}{\partial z} + \frac{\partial w}{\partial y}\right)\frac{\partial \nu}{\partial z}\right] + (1/Fr^2)g_y \end{aligned} \tag{11}$$

$$\begin{aligned} N_3 = & -\frac{\partial (uw)}{\partial x} - \frac{\partial (vw)}{\partial y} - \frac{\partial (w^2)}{\partial z} + \frac{1}{Re}\nu(q)\left[\frac{\partial^2 w}{\partial x^2} + \frac{\partial^2 w}{\partial y^2} + \frac{\partial^2 w}{\partial z^2}\right] \\ & + \frac{1}{Re}\left[\left(\frac{\partial u}{\partial z} + \frac{\partial w}{\partial x}\right)\frac{\partial \nu}{\partial x} + \left(\frac{\partial v}{\partial z} + \frac{\partial w}{\partial y}\right)\frac{\partial \nu}{\partial y} + 2\frac{\partial w}{\partial z}\frac{\partial \nu}{\partial z}\right] + (1/Fr^2)g_z \end{aligned} \tag{12}$$

where $Re = UL/\nu$ and $Fr = U/\sqrt{Lg}$ are the associated Reynolds number and Froude number respectively.

The local shear rate (4) is given by

$$q = \left[2\left(\frac{\partial u}{\partial x}\right)^2 + 2\left(\frac{\partial v}{\partial y}\right)^2 + 2\left(\frac{\partial w}{\partial z}\right)^2 + \left(\frac{\partial u}{\partial y} + \frac{\partial v}{\partial x}\right)^2 + \left(\frac{\partial u}{\partial z} + \frac{\partial w}{\partial x}\right)^2 + \left(\frac{\partial v}{\partial z} + \frac{\partial w}{\partial y}\right)^2\right]^{1/2}. \tag{13}$$

The viscosity $\nu(q)$ can be any function of q representing the shear-thinning nature. In the simulations presented in this paper we employed the Cross model:

$$\nu(q) = \nu_\infty + \frac{\nu_0 - \nu_\infty}{(1 + (Kq)^m)} \tag{14}$$

where m, ν_0, ν_∞ and K are given positive constants.

3. Procedure

To solve equations (8) and (9) we employ the following procedure which is the 3D-version of GENSMAC (see Tomé et al. (1996)).

Let us suppose that at a given time, say t_0, the velocity field $\mathbf{u}(\mathbf{x}, t_0)$ is known and boundary conditions for the velocity and pressure are given. To compute the velocity field and the pressure field at the advanced time $t = t_0 + \delta t$, we proceed as follows:

Step 1: Compute $q(x, y, z, t_0)$ and $\nu(x, y, z, t_0)$ using $\mathbf{u}(x, y, z, t_0)$

Step 2: Let $\widetilde{p}(x, y, z, t)$ be a pressure field which satisfies the correct pressure condition on the free surface.

Step 3: Calculate the intermediate velocity field, $\widetilde{\mathbf{u}}(x, y, z, t)$, from

$$\frac{\partial \widetilde{\mathbf{u}}}{\partial t} = -\nabla \widetilde{p} + N(\mathbf{u}) \tag{15}$$

with $\widetilde{\mathbf{u}}(x, y, z, t_0) = \mathbf{u}(x, y, z, t_0)$ using the correct boundary conditions for $\mathbf{u}(x, y, z, t_0)$. The components of $N(\mathbf{u})$ are defined by (10)–(12). These equations are solved by an explicit finite difference method.

Step 4: Solve the Poisson equation

$$\nabla^2 \psi(x, y, z, t) = \nabla . \widetilde{\mathbf{u}}(x, y, z, t). \tag{16}$$

The appropriate boundary conditions for this equation are (see Tomé et al. (1996))

$$\frac{\partial \psi}{\partial n} = 0 \qquad \text{on rigid boundaries and} \qquad \psi = 0 \qquad \text{on the free surface.}$$

Step 4: Compute the velocity field

$$\mathbf{u}(x, y, z, t) = \widetilde{\mathbf{u}}(x, y, z, t) - \nabla \psi(x, y, z, t). \tag{17}$$

Step 5: Compute the pressure

$$p(x, y, z, t) = \widetilde{p}(x, y, z, t_0) + \frac{\psi(x, y, z, t)}{\delta t}. \tag{18}$$

Thus, we solve the momentum equations explicitly followed by a sparse symmetric system (the discrete Poisson equation) for the potential function ψ. For container filling problems the order of this system is continually increasing (since one only solves for $\mathbf{u}$ and p within the bulk fluid).

Boundary conditions

The rigid boundary conditions currently implemented are of no-slip and prescribed inflow types. They are applied on the rigid boundaries (containers and inflow boundaries) in contact with the fluid and require the calculation of the intersections of lines parallel to the sides of the cells with the containers. These intersections are calculated only once and stored in a tree structure representing the cells in the structures Container and Inflow. For details see Castelo et al. [2].

4. Basic Finite Difference Equations

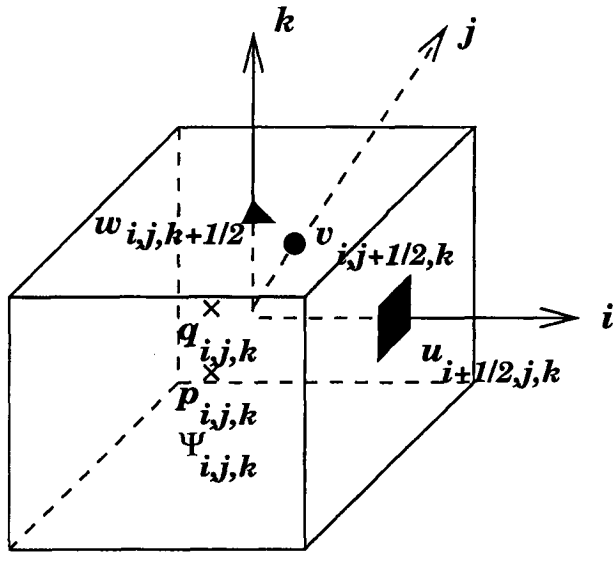

Fig. 1. Typical cell used in a calculational time-step.

In order to solve **Steps 1 to 5** of the procedure presented in the Section 3 we employ the following approach. A staggered grid is used and a typical cell is shown in figure 1. The variables $p_{i,j,k}$, the potential function $\psi_{i,j,k}$ and the discrete shear rate $q_{i,j,k}$ are positioned at a cell centre while $u_{i,j,k}$, $v_{i,j,k}$ and $w_{i,j,k}$ are staggered by a translation of $\delta x/2$, $\delta y/2$ and $\delta z/2$ respectively. A scheme for identifying the free surface and the fluid region is employed. To accommodate this, the cells within the mesh are defined as full cells (F), surface cells (S), empty cells (E) and boundary cells (B). A detailed description of these is given in Tomé et al. [20].

The momentum equation (15) is discretized and applied at $u-$nodes, $v-$nodes and $w-$nodes respectively. The time derivative is discretized explicitly while the Laplacian is approximated by central differences. The convective terms are approximated by a high order upwind scheme namely, the VONOS method (see Varonos and Bergeles [24]). Details of these approximations are given in Ferreira et al. [7]. For the sake of clarity we shall present the approximations of the derivatives appearing in the non-Newtonian terms of (15) together with the approximations for the computation of the local shear rate $q_{i,j,k}$ and the ν-derivatives.

For instance, considering equation (15) for $\widetilde{u}$, the discretization of the non-Newtonian terms is performed as follows: the $u-$derivatives are approximated by central differences while for the $v-$ and $w-$derivatives we first compute an average and then apply central differences, giving

$$
\begin{aligned}
\left[\frac{\partial u}{\partial x}\right]_{i+\frac{1}{2},j,k} &= \frac{u_{i+\frac{3}{2},j,k} - u_{i-\frac{1}{2},j,k}}{2\delta x}, \\
\left[\frac{\partial u}{\partial y}\right]_{i+\frac{1}{2},j,k} &= \frac{u_{i+\frac{1}{2},j+1,k} - u_{i+\frac{1}{2},j-1,k}}{2\delta y}, \\
\left[\frac{\partial u}{\partial z}\right]_{i+\frac{1}{2},j,k} &= \frac{u_{i+\frac{1}{2},j,k+1} - u_{i+\frac{1}{2},j,k-1}}{2\delta z}, \\
\left[\frac{\partial v}{\partial x}\right]_{i+\frac{1}{2},j,k} &= \frac{v_{i+1,j+\frac{1}{2},k} + v_{i+1,j-\frac{1}{2},k} - v_{i,j+\frac{1}{2},k} - v_{i,j-\frac{1}{2},k}}{2\delta x}, \\
\left[\frac{\partial w}{\partial x}\right]_{i+\frac{1}{2},j,k} &= \frac{w_{i+1,j,k+\frac{1}{2}} + w_{i+1,j,k-\frac{1}{2}} - w_{i,j,k+\frac{1}{2}} - w_{i,j,k-\frac{1}{2}}}{2\delta x},
\end{aligned}
$$

respectively. The computation of the shear rate is given next.

4.1 Calculation of the discrete shear rate $q_{i,j,k}$ on full cells

The shear rate evaluated at $(i\delta x, j\delta y, k\delta z)$ is:

$$
\begin{aligned}
q_{i,j,k} = \Bigg(& 2\left[\frac{\partial u}{\partial x}\right]^2_{i,j,k} + 2\left[\frac{\partial v}{\partial y}\right]^2_{i,j,k} + 2\left[\frac{\partial w}{\partial z}\right]^2_{i,j,k} + \left[\frac{\partial u}{\partial y} + \frac{\partial v}{\partial x}\right]^2_{i,j,k} + \left[\frac{\partial u}{\partial z} + \frac{\partial w}{\partial x}\right]^2_{i,j,k} \\
& + \left[\frac{\partial v}{\partial z} + \frac{\partial w}{\partial y}\right]^2_{i,j,k} \Bigg)^{1/2}. \qquad (19)
\end{aligned}
$$

The derivatives $\left[\frac{\partial u}{\partial x}\right]_{i,j,k}$, $\left[\frac{\partial v}{\partial y}\right]_{i,j,k}$ and $\left[\frac{\partial w}{\partial z}\right]_{i,j,k}$ are approximated by central differences, namely

$$
\left[\frac{\partial u}{\partial x}\right]_{i,j,k} = \frac{u_{i+\frac{1}{2},j,k} - u_{i-\frac{1}{2},j,k}}{\delta x}, \quad \left[\frac{\partial v}{\partial y}\right]_{i,j,k} = \frac{v_{i,j+\frac{1}{2},k} - v_{i,j-\frac{1}{2},k}}{\delta y}, \quad \left[\frac{\partial v}{\partial y}\right]_{i,j,k} = \frac{w_{i,j,k+\frac{1}{2}} - w_{i,j,k-\frac{1}{2}}}{\delta z}.
$$

To approximate the cross derivatives in (19) we first average and then apply central differences. For instance, the derivatives $\left[\frac{\partial u}{\partial y}\right]_{i,j,k}$ and $\left[\frac{\partial u}{\partial z}\right]_{i,j,k}$ are approximated by

$$
\left[\frac{\partial u}{\partial y}\right]_{i,j,k} = \frac{u_{i,j+\frac{1}{2},k} - u_{i,j-\frac{1}{2},k}}{\delta y} \quad \text{and} \quad \left[\frac{\partial u}{\partial z}\right]_{i,j,k} = \frac{u_{i,j,k+\frac{1}{2}} - u_{i,j,k-\frac{1}{2}}}{\delta z}
$$

where

$$
\begin{aligned}
u_{i,j+\frac{1}{2},k} &= \frac{u_{i+\frac{1}{2},j,k} + u_{i-\frac{1}{2},j,k} + u_{i+\frac{1}{2},j+1,k} + u_{i-\frac{1}{2},j+1,k}}{4} \\
u_{i,j-\frac{1}{2},k} &= \frac{u_{i+\frac{1}{2},j,k} + u_{i-\frac{1}{2},j,k} + u_{i+\frac{1}{2},j-1,k} + u_{i-\frac{1}{2},j-1,k}}{4} \\
u_{i,j,k+\frac{1}{2}} &= \frac{u_{i+\frac{1}{2},j,k} + u_{i-\frac{1}{2},j,k} + u_{i+\frac{1}{2},j,k+1} + u_{i-\frac{1}{2},j,k+1}}{4} \\
u_{i,j,k-\frac{1}{2}} &= \frac{u_{i+\frac{1}{2},j,k} + u_{i-\frac{1}{2},j,k} + u_{i+\frac{1}{2},j,k-1} + u_{i-\frac{1}{2},j,k-1}}{4}
\end{aligned}
$$

The other derivatives (e.g. $\left[\frac{\partial v}{\partial x}\right]_{i,j,k}$, $\left[\frac{\partial v}{\partial z}\right]_{i,j,k}$, $\cdots$, etc) are obtained similarly.

Equation (19) is applied at every full cell; the shear rate on surface cells is computed according to the equations presented in Section 4.4.

4.2 Computation of ν–derivatives

Once the discrete shear rate (19) has been computed for every full and surface cell, the ν–derivatives appearing in (10)–(12) are computed as follows:

Consider equation (15) for the calculation of $\widetilde{u}$. In this case, the derivative $\left[\frac{\partial \nu}{\partial x}\right]_{i+\frac{1}{2},j,k}$ is approximated by

$$
\left[\frac{\partial \nu}{\partial x}\right]_{i+\frac{1}{2},j,k} = \frac{\nu(q_{i+1,j,k}) - \nu(q_{i,j,k})}{\delta x}.
$$

To evaluate the derivatives $\left[\frac{\partial \nu}{\partial y}\right]_{i+\frac{1}{2},j,k}$ and $\left[\frac{\partial \nu}{\partial z}\right]_{i+\frac{1}{2},j,k}$ we first average q on mesh corners and then apply central differences, namely,

$$
\left[\frac{\partial \nu}{\partial y}\right]_{i+\frac{1}{2},j,k} = \frac{\nu(q_{i+\frac{1}{2},j+\frac{1}{2},k}) - \nu(q_{i+\frac{1}{2},j-\frac{1}{2},k})}{\delta y}
$$

and

$$
\left[\frac{\partial \nu}{\partial z}\right]_{i+\frac{1}{2},j,k} = \frac{\nu(q_{i+\frac{1}{2},j,k+\frac{1}{2}}) - \nu(q_{i+\frac{1}{2},j,k-\frac{1}{2}})}{\delta z}
$$

where

$$
\begin{aligned}
q_{i+\frac{1}{2},j+\frac{1}{2},k} &= \frac{q_{i,j,k} + q_{i+1,j,k} + q_{i,j+1,k} + q_{i+1,j+1,k}}{4} \\
q_{i+\frac{1}{2},j-\frac{1}{2},k} &= \frac{q_{i,j,k} + q_{i+1,j,k} + q_{i,j-1,k} + q_{i+1,j-1,k}}{4} \\
q_{i+\frac{1}{2},j,k+\frac{1}{2}} &= \frac{q_{i,j,k} + q_{i+1,j,k} + q_{i,j,k+1} + q_{i+1,j,k+1}}{4} \\
q_{i+\frac{1}{2},j,k-\frac{1}{2}} &= \frac{q_{i,j,k} + q_{i+1,j,k} + q_{i,j,k-1} + q_{i+1,j,k-1}}{4}.
\end{aligned}
$$

However, if the corner cell, let us say $(i+\frac{1}{2}, j+\frac{1}{2}, k)$, is situated on an edge which is shared by a boundary cell or an empty cell then these derivatives are calculated by using a forward or a backward difference. For instance, let us consider the cells in figure 2a. In this case, the value of $\left[\frac{\partial \nu}{\partial y}\right]_{i+\frac{1}{2},j,k}$ is computed by

$$\left[\frac{\partial \nu}{\partial y}\right]_{i+\frac{1}{2},j,k} = \frac{\nu(q_{i+\frac{1}{2},j,k}) - \nu(q_{i+\frac{1}{2},j-1,k})}{\delta y}$$

where

$$q_{i+\frac{1}{2},j,k} = \frac{q_{i,j,k} + q_{i+1,j,k}}{2} \text{ and } q_{i+\frac{1}{2},j-1,k} = \frac{q_{i,j-1,k} + q_{i+1,j-1,k}}{2}.$$

Similarly, the value of $\left[\frac{\partial \nu}{\partial z}\right]_{i+\frac{1}{2},j,k}$ (see figure 2b) is given by

$$\left[\frac{\partial \nu}{\partial z}\right]_{i+\frac{1}{2},j,k} = \frac{\nu(q_{i+\frac{1}{2},j,k}) - \nu(q_{i+\frac{1}{2},j,k-1})}{\delta y}$$

where

$$q_{i+\frac{1}{2},j,k} = \frac{q_{i,j,k} + q_{i+1,j,k}}{2} \text{ and } q_{i+\frac{1}{2},j,k-1} = \frac{q_{i,j,k-1} + q_{i+1,j,k-1}}{2}.$$

Other situations of cells having one of the corners lying on edges shared by boundary or empty cells are handled in a similar manner.

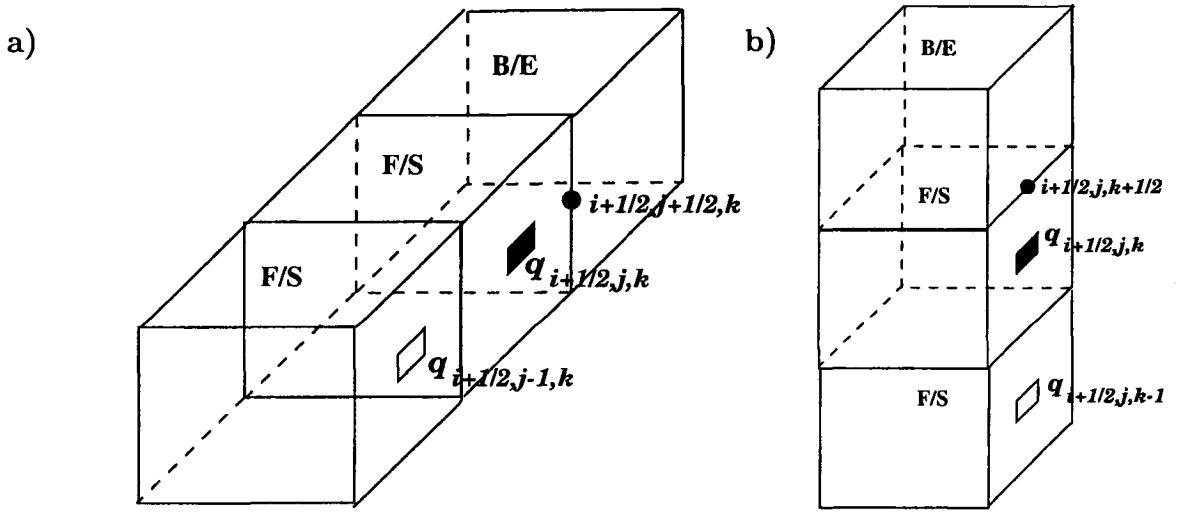

Fig. 2. Calculation of the shear rate on a cell near an E or B-cell.

The approximation of the derivatives appearing in equations (11) and (12) are handled similarly.

4.3 Computation of $\nu(q)$

The values of the viscosity $\nu(q)$ is required at $u-$, $v-$ and $w-$nodes and at cell centres. These can be obtained from (14). For instance, if we use the Cross model (14) then

$$\nu(q_{i,j,k}) = \nu_\infty + \frac{\nu_0 - \nu_\infty}{1 + (Kq_{i,j,k})^m} \,. \tag{20}$$

Therefore, equation (15) is approximated by the following difference equations

$$\begin{aligned}
\widetilde{u}_{i+\frac{1}{2},j,k} = u_{i+\frac{1}{2},j,k} + \delta t \Bigg[& -\mathbf{conv}(u^2) - \mathbf{conv}(vu) - \mathbf{conv}(wu) + \frac{\widetilde{p}_{i+1,j,k} - \widetilde{p}_{i,j,k}}{\delta x} + \frac{1}{Fr^2} g_x \\
& + \frac{1}{Re} \nu(q_{i+\frac{1}{2},j,k}) \Bigg(\frac{u_{i-\frac{1}{2},j,k} - 2u_{i+\frac{1}{2},j,k} + u_{i+\frac{3}{2},j,k}}{\delta x^2} + \frac{u_{i+\frac{1}{2},j-1,k} - 2u_{i+\frac{1}{2},j,k} + u_{i+\frac{1}{2},j+1,k}}{\delta y^2} \\
& \frac{u_{i+\frac{1}{2},j,k-1} - 2u_{i+\frac{1}{2},j,k} + u_{i+\frac{1}{2},j,k+1}}{\delta z^2} \Bigg) + \frac{1}{Re} \Bigg(\left(\frac{u_{i+\frac{3}{2},j,k} - u_{i-\frac{1}{2},j,k}}{\delta x} \right) \frac{\partial \nu(q)}{\partial x}|_{i+\frac{1}{2},j,k} \\
& + \left(\frac{u_{i+\frac{1}{2},j+1,k} - u_{i+\frac{1}{2},j-1,k}}{2\delta y} + \frac{v_{i+1,j+\frac{1}{2},k} + v_{i+1,j-\frac{1}{2},k} - v_{i,j+\frac{1}{2},k} - v_{i,j-\frac{1}{2},k}}{2\delta x} \right) \frac{\partial \nu(q)}{\partial y}|_{i+\frac{1}{2},j,k} \\
& + \left(\frac{u_{i+\frac{1}{2},j,k+1} - u_{i+\frac{1}{2},j,k-1}}{2\delta z} + \frac{w_{i+1,j,k+\frac{1}{2}} + w_{i+1,j,k-\frac{1}{2}} - w_{i,j,k+\frac{1}{2}} - w_{i,j,k-\frac{1}{2}}}{2\delta x} \right) \frac{\partial \nu(q)}{\partial z}|_{i+\frac{1}{2},j,k} \Bigg) \Bigg]
\end{aligned} \tag{21}$$

$$\begin{aligned}
\widetilde{v}_{i,j+\frac{1}{2},k} = v_{i,j+\frac{1}{2},k} + \delta t \Bigg[& -\mathbf{conv}(uv) - \mathbf{conv}(v^2) - \mathbf{conv}(wv) + \frac{\widetilde{p}_{i,j+1,k} - \widetilde{p}_{i,j,k}}{\delta y} + \frac{1}{Fr^2} g_y \\
& + \frac{1}{Re} \nu(q_{i,j+\frac{1}{2},k}) \Bigg(\frac{v_{i-1,j+\frac{1}{2},k} - 2v_{i,j+\frac{1}{2},k} + v_{i+1,j+\frac{1}{2},k}}{\delta x^2} + \frac{v_{i,j-\frac{1}{2},k} - 2v_{i,j+\frac{1}{2},k} + v_{i,j+\frac{3}{2},k}}{\delta y^2} \\
& + \frac{v_{i,j+\frac{1}{2},k-1} - 2v_{i,j+\frac{1}{2},k} + v_{i,j+\frac{1}{2},k+1}}{\delta z^2} \Bigg) + \frac{1}{Re} \Bigg(\left(\frac{u_{i+\frac{1}{2},j+1,k} + u_{i-\frac{1}{2},j+1,k} - u_{i+\frac{1}{2},j,k} - u_{i-\frac{1}{2},j,k}}{2\delta y} \right. \\
& \left. + \frac{v_{i+1,j+\frac{1}{2},k} - v_{i-1,j+\frac{1}{2},k}}{2\delta x} \right) \frac{\partial \nu(q)}{\partial x}|_{i,j+\frac{1}{2},k} + \left(\frac{v_{i,j+\frac{3}{2},k} - v_{i,j-\frac{1}{2},k}}{\delta y} \right) \frac{\partial \nu(q)}{\partial y}|_{i,j+\frac{1}{2},k} \\
& + \left(\frac{v_{i,j+\frac{1}{2},k+1} - v_{i,j+\frac{1}{2},k-1}}{2\delta z} + \frac{w_{i,j+1,k+\frac{1}{2}} + w_{i,j+1,k-\frac{1}{2}} - w_{i,j,k+\frac{1}{2}} - w_{i,j,k-\frac{1}{2}}}{2\delta y} \right) \frac{\partial \nu(q)}{\partial z}|_{i,j+\frac{1}{2},k} \Bigg) \Bigg]
\end{aligned} \tag{22}$$

$$\begin{aligned}
\widetilde{w}_{i,j,k+\frac{1}{2}} = w_{i,j,k+\frac{1}{2}} + \delta t \Bigg[& -\mathbf{conv}(uw) - \mathbf{conv}(vw) - \mathbf{conv}(w^2) \frac{\widetilde{p}_{i,j,k+1} - \widetilde{p}_{i,j,k}}{\delta z} + \frac{1}{Fr^2} g_z \\
& + \frac{1}{Re} \nu(q_{i,j,k+\frac{1}{2}}) \Bigg(\frac{w_{i-1,j,k+\frac{1}{2}} - 2w_{i,j,k+\frac{1}{2}} + w_{i+1,j,k+\frac{1}{2}}}{\delta x^2} + \frac{w_{i,j-1,k+\frac{1}{2}} - 2w_{i,j,k+\frac{1}{2}} + w_{i,j+1,k+\frac{1}{2}}}{\delta y^2} \\
& + \frac{w_{i,j,k-\frac{1}{2}} - 2w_{i,j,k+\frac{1}{2}} + w_{i,j,k+\frac{3}{2}}}{\delta z^2} \Bigg) - \frac{1}{Re} \Bigg(\left(\frac{u_{i+\frac{1}{2},j,k+1} + u_{i-\frac{1}{2},j,k+1} - u_{i+\frac{1}{2},j,k} - u_{i-\frac{1}{2},j,k}}{\delta x} \right. \\
& \left. \frac{w_{i+1,j,k+\frac{1}{2}} - w_{i-1,j,k-\frac{1}{2}}}{2\delta x} \right) \frac{\partial \nu(q)}{\partial x}|_{i,j,k+\frac{1}{2}} + \left(\frac{v_{i,j+\frac{1}{2},k+1} + v_{i,j-\frac{1}{2},k+1} - v_{i,j+\frac{1}{2},k} - v_{i,j-\frac{1}{2},k}}{2\delta z} \right. \\
& \left. + \frac{w_{i,j+1,k+\frac{1}{2}} - w_{i,j-1,k-\frac{1}{2}}}{2\delta y} \right) \frac{\partial \nu(q)}{\partial y}|_{i,j,k+\frac{1}{2}} + \left(\frac{w_{i,j,k+\frac{3}{2}} - w_{i,j,k-\frac{1}{2}}}{\delta z} \right) \frac{\partial \nu(q)}{\partial z}|_{i,j,k+\frac{1}{2}} \Bigg) \Bigg]
\end{aligned} \tag{23}$$

Approximations of the viscosity and the shear rate on surface cells will be given in the next section.

The Poisson equation (18) is discretized at cell centres using the seven-point Laplacian, namely,

$$\frac{\psi_{i+1,j,k} - 2\psi_{i,j,k} + \psi_{i-1,j,k}}{\delta x^2} + \frac{\psi_{i,j+1,k} - 2\psi_{i,j,k} + \psi_{i,j-1,k}}{\delta y^2} + \frac{\psi_{i,j,k+1} - 2\psi_{i,j,k} + \psi_{i,j,k-1}}{\delta z^2} = \widetilde{D}_{i,j,k} \tag{24}$$

where

$$\widetilde{D}_{i,j,k} = \frac{\widetilde{u}_{i+\frac{1}{2},j,k} - \widetilde{u}_{i-\frac{1}{2},j,k}}{\delta x} + \frac{\widetilde{v}_{i,j+\frac{1}{2},k} - \widetilde{v}_{i,j-\frac{1}{2},k}}{\delta y} + \frac{\widetilde{w}_{i,j,k+\frac{1}{2}} - \widetilde{w}_{i,j,k-\frac{1}{2}}}{\delta z} .$$

Equation (24) leads to a symmetric and positive definite linear system for $\psi_{i,j,k}$. In order to solve this linear system we employ the conjugate gradient method as implemented in GENSMAC (see Tome and McKee [21]). Thus, a calculational cycle consists of solving equations (21)–(23) and (24) sequentially for a given time step.

4.4 Approximate Free Surface Stress Conditions

Let **n**, **m1**, and **m2** denote unit normal and tangential vectors at the free surface. Then, the boundary conditions (7) may be written as

$$p - \frac{2}{Re}\nu(q)\left[\frac{\partial u}{\partial x}n_x^2 + \frac{\partial v}{\partial y}n_y^2 + \frac{\partial w}{\partial z}n_z^2 + \left(\frac{\partial u}{\partial y} + \frac{\partial v}{\partial x}\right)n_x n_y + \left(\frac{\partial u}{\partial z} + \frac{\partial w}{\partial x}\right)n_x n_z + \left(\frac{\partial v}{\partial z} + \frac{\partial w}{\partial y}\right)n_y n_z\right] = 0\ , \tag{25}$$

$$\frac{1}{Re}\left[2\frac{\partial u}{\partial x}m1_x n_x + 2\frac{\partial v}{\partial y}m1_y n_y + 2\frac{\partial w}{\partial z}m1_z n_z + \left(\frac{\partial u}{\partial y} + \frac{\partial v}{\partial x}\right)(m1_x n_y + m1_y n_x) + \left(\frac{\partial u}{\partial z} + \frac{\partial w}{\partial x}\right)(m1_x n_z + m1_z n_x) + \left(\frac{\partial v}{\partial z} + \frac{\partial w}{\partial y}\right)(m1_y n_z + m1_z n_y)\right] = 0\ , \tag{26}$$

$$\frac{1}{Re}\left[2\frac{\partial u}{\partial x}m2_x n_x + 2\frac{\partial v}{\partial y}m2_y n_y + 2\frac{\partial w}{\partial z}m2_z n_z + \left(\frac{\partial u}{\partial y} + \frac{\partial v}{\partial x}\right)(m2_x n_y + m2_y n_x) + \left(\frac{\partial u}{\partial z} + \frac{\partial w}{\partial x}\right)(m2_x n_z + m2_z n_x) + \left(\frac{\partial v}{\partial z} + \frac{\partial w}{\partial y}\right)(m2_y n_z + m2_z n_y)\right] = 0\ , \tag{27}$$

respectively. In order to apply these conditions we employ an extension of the ideas suggested by Tomé et al. [18]. Let us suppose that the mesh spacing is small enough so that, locally, the free surface can be approximated by a planar surface. Then (25)–(27) can be approximated by local finite differences. There are essentially three cases: planar surface parallel to a coordinate axis; a 45^0-sloped surface; and a 60^0 sloped planar surface. Equations (26) and (27) do not involve $\nu(q)$ and have been dealt with fully in Tomé et al. [20]. However, the calculation of the pressure on these planar surfaces requires the discretization of q and thus $\nu(q)$ for the three cases. These now follow.

4.4.1 Planar surface parallel to a coordinate axis: This surface is defined to have the normal vector in the direction of one of the coordinate directions i.e. $\mathbf{n} = (n_x, 0, 0)$ or $\mathbf{n} = (0, n_y, 0)$ or $\mathbf{n} = (0, 0, n_z)$. These surfaces are identified by surface cells having only one face in contact with one empty cell face (see figure 3a).

It can be seen that on such surfaces conditions (25)–(27) may be written as

$$p - \frac{2}{Re}\nu(q)\left[\frac{\partial u}{\partial x}n_x^2 + \frac{\partial v}{\partial y}n_y^2 + \frac{\partial w}{\partial z}n_z^2\right] = 0, \tag{28}$$

$$\frac{1}{Re}\left[\left(\frac{\partial u}{\partial y} + \frac{\partial v}{\partial x}\right)n_x + \left(\frac{\partial v}{\partial z} + \frac{\partial w}{\partial y}\right)n_y + \left(\frac{\partial u}{\partial z} + \frac{\partial w}{\partial x}\right)n_z\right] = 0\ , \tag{29}$$

$$\frac{1}{Re}\left[\left(\frac{\partial u}{\partial z} + \frac{\partial w}{\partial x}\right)n_x + \left(\frac{\partial u}{\partial y} + \frac{\partial v}{\partial x}\right)n_y + \left(\frac{\partial v}{\partial z} + \frac{\partial w}{\partial y}\right)n_z\right] = 0\ , \tag{30}$$

respectively.

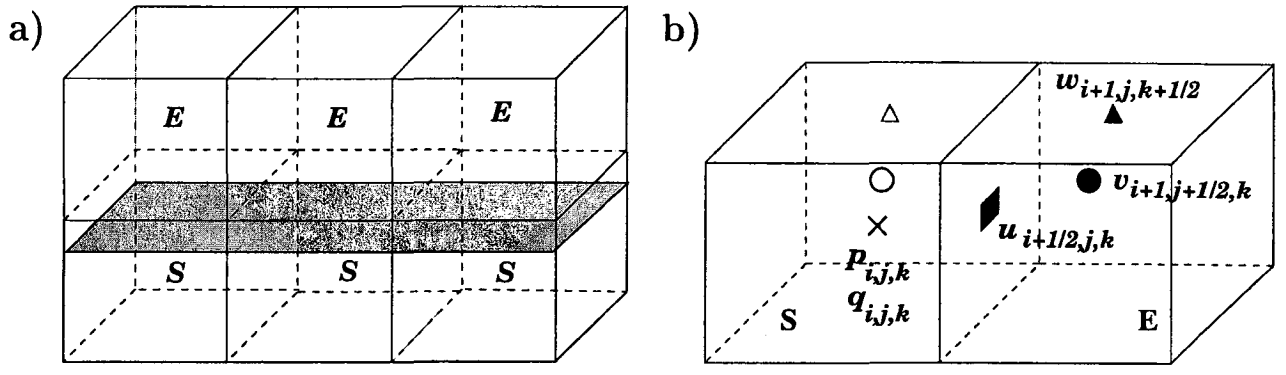

Fig. 3. S–cells having only one face in contact with one E–cell face.

Equation (28) can be approximated by finite differences in a straight forward manner. For instance, consider the surface cell in figure 3b. For this cell we assume that the outward normal vector is pointing to the E-cell in which case we take $\mathbf{n} = (1, 0, 0)$. Equations (28)–(30) then reduce to

$$p = \frac{2}{Re}\nu(q)\left(\frac{\partial u}{\partial x}\right) , \tag{31}$$

$$\left(\frac{\partial u}{\partial y} + \frac{\partial v}{\partial x}\right) = 0 , \tag{32}$$

$$\left(\frac{\partial u}{\partial z} + \frac{\partial w}{\partial x}\right) = 0 . \tag{33}$$

To compute $\nu(q_{i,j,k})$ we first calculate the shear rate (13) which in these cells reduces to (using (32) and (33))

$$q = \left[2\left(\frac{\partial u}{\partial x}\right)^2 + 2\left(\frac{\partial v}{\partial y}\right)^2 + 2\left(\frac{\partial w}{\partial z}\right)^2 + \left(\frac{\partial v}{\partial z} + \frac{\partial w}{\partial y}\right)^2\right]^{1/2}$$

and is approximated by

$$q_{i,j,k} = \left[2\left(\left(\frac{u_{i+\frac{1}{2},j,k} - u_{i-\frac{1}{2},j,k}}{\delta x}\right)^2 + \left(\frac{v_{i,j+\frac{1}{2},k} - v_{i,j-\frac{1}{2},k}}{\delta y}\right)^2 + \left(\frac{w_{i,j,k+\frac{1}{2}} - w_{i,j,k-\frac{1}{2}}}{\delta z}\right)^2\right) + \left(\frac{v_{i,j,k+\frac{1}{2}} - v_{i,j,k-\frac{1}{2}}}{\delta z} + \frac{w_{i,j+\frac{1}{2},k} - w_{i,j-\frac{1}{2},k}}{\delta y}\right)^2\right]^{1/2}$$

where

$$v_{i,j,k+\frac{1}{2}} = \frac{v_{i,j+\frac{1}{2},k} + v_{i,j-\frac{1}{2},k} + v_{i,j+\frac{1}{2},k+1} + v_{i,j-\frac{1}{2},k+1}}{4}$$

$$v_{i,j,k-\frac{1}{2}} = \frac{v_{i,j+\frac{1}{2},k} + v_{i,j-\frac{1}{2},k} + v_{i,j+\frac{1}{2},k-1} + v_{i,j-\frac{1}{2},k-1}}{4}$$

$$w_{i,j+\frac{1}{2},k} = \frac{w_{i,j,k+\frac{1}{2}} + w_{i,j,k-\frac{1}{2}} + w_{i,j+1,k+\frac{1}{2}} + w_{i,j+1,k-\frac{1}{2}}}{4}$$

$$w_{i,j-\frac{1}{2},k} = \frac{w_{i,j,k+\frac{1}{2}} + w_{i,j,k-\frac{1}{2}} + w_{i,j-1,k+\frac{1}{2}} + w_{i,j-1,k-\frac{1}{2}}}{4}$$

The viscosity is then evaluated by

$$\nu(q_{i,j,k}) = \nu_\infty + \frac{\nu_0 - \nu_\infty}{1 + (Kq_{i,j,k})^m} .$$

The pressure $\widetilde{p}_{i,j,k}$ for the surface cell is then computed using (31) applied at the cell centre yielding

$$\widetilde{p}_{i,j,k} = \frac{2}{Re}\nu(q_{i,j,k}) \left(\frac{u_{i+\frac{1}{2},j,k} - u_{i-\frac{1}{2},j,k}}{\delta x} \right) .$$

Other configurations of surface cells having only one face in contact with an empty cell face are treated similarly.

4.4.2 45^0–sloped planar surface: These surfaces are defined to have the local unit normal vector making $\mathbf{45^0}$ with two adjacent coordinate axes (see figure 4). They are identified by surface cells having two adjacent faces contiguous with empty cell faces. On such surfaces we assume the unit normal vector takes the form $\mathbf{n} = \left(\pm\frac{\sqrt{2}}{2}, \pm\frac{\sqrt{2}}{2}, 0\right)$ or $\mathbf{n} = \left(\pm\frac{\sqrt{2}}{2}, 0, \pm\frac{\sqrt{2}}{2}\right)$ or $\mathbf{n} = \left(0, \pm\frac{\sqrt{2}}{2}, \pm\frac{\sqrt{2}}{2}\right)$. It can be seen that there are 12 different possible $\mathbf{45^0}$–sloped planar surfaces. The pressure condition approximation for one particular case will be given here; the remaining cases are treated similarly. Details of the equations involved for each case can be found in Tomé et al. [20].

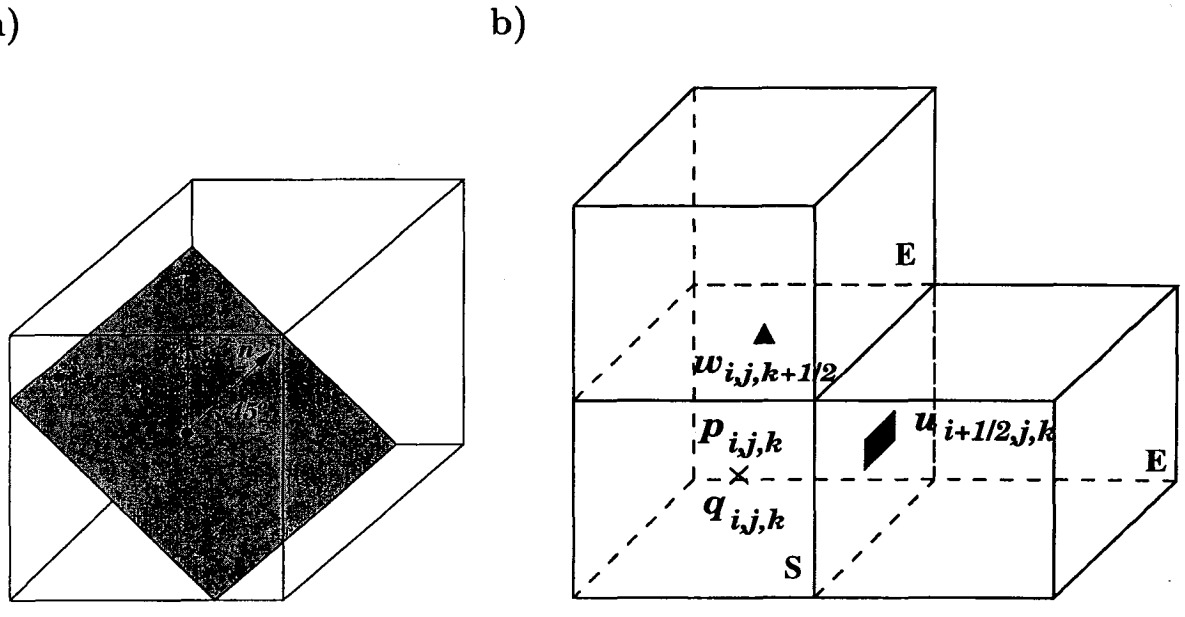

Fig. 4. Example of a 45^0–sloped planar surface.

Let us consider the surface cell in figure 4b. For this cell we take $\mathbf{n} = \left(\frac{\sqrt{2}}{2}, 0, \frac{\sqrt{2}}{2}\right)$ and the tangential vectors are chosen to be $\mathbf{m1} = \left(\frac{\sqrt{2}}{2}, 0, -\frac{\sqrt{2}}{2}\right)$ and $\mathbf{m2} = (0, 1, 0)$.

Introducing these vectors into the stress conditions (25)–(27) yields

$$p = \frac{1}{Re}\nu(q)\left(\frac{\partial u}{\partial x} + \frac{\partial w}{\partial z} + \frac{\partial u}{\partial z} + \frac{\partial w}{\partial x}\right) , \tag{35}$$

$$\left(\frac{\partial u}{\partial y} + \frac{\partial v}{\partial x}\right) + \left(\frac{\partial v}{\partial z} + \frac{\partial w}{\partial y}\right) = 0 , \tag{36}$$

$$\frac{\partial u}{\partial x} - \frac{\partial w}{\partial z} = 0 , \tag{37}$$

respectively. The values of $u_{i+\frac{1}{2},j,k}$ and $w_{i,j,k+\frac{1}{2}}$ at empty-cell faces are required. These are obtained by applying (37) and the mass conservation equation (9) at the surface cell centre. Details of the finite difference equations for calculating $u_{i+\frac{1}{2},j,k}$ and $w_{i,j,k+\frac{1}{2}}$ are presented in Tomé et al. [20].

Calculation of $q_{i,j,k}$

By using (36) and (37), the shear rate (13) in these cells reduces to

$$q = \left(4\left[\frac{\partial u}{\partial x}\right]^2 + 2\left[\frac{\partial v}{\partial y}\right]^2 + 2\left[\frac{\partial u}{\partial y} + \frac{\partial v}{\partial x}\right]^2 + \left[\frac{\partial u}{\partial z} + \frac{\partial w}{\partial x}\right]^2\right)^{1/2} . \tag{38}$$

The derivatives $\left[\frac{\partial u}{\partial x}\right]_{i,j,k}$, and $\left[\frac{\partial v}{\partial y}\right]_{i,j,k}$ are approximated by central differences in a manner similar to those for the full cells. The cross derivative $\left[\frac{\partial u}{\partial y}\right]_{i,j,k}$ is also approximated by central differences and is given by

$$\left[\frac{\partial u}{\partial y}\right]_{i,j,k} = \frac{u_{i,j+\frac{1}{2},k} - u_{i,j-\frac{1}{2},k}}{\delta y}$$

where

$$u_{i,j+\frac{1}{2},k} = \frac{u_{i+\frac{1}{2},j,k} + u_{i-\frac{1}{2},j,k} + u_{i+\frac{1}{2},j+1,k} + u_{i-\frac{1}{2},j+1,k}}{4} ,$$

$$u_{i,j-\frac{1}{2},k} = \frac{u_{i+\frac{1}{2},j,k} + u_{i-\frac{1}{2},j,k} + u_{i+\frac{1}{2},j-1,k} + u_{i-\frac{1}{2},j-1,k}}{4} .$$

However, for the cross derivative $\left[\frac{\partial u}{\partial z}\right]_{i,j,k}$ we average and then employ either a forward difference or a backward difference. The backward and the forward differences are applied according to the configuration of the surface cells. For instance, if we consider the surface cell shown in figure 4a then the derivative $\left[\frac{\partial u}{\partial z}\right]_{i,j,k}$ is computed by

$$\left[\frac{\partial u}{\partial z}\right]_{i,j,k} = \frac{u_{i+\frac{1}{2},j,k} + u_{i-\frac{1}{2},j,k} - u_{i+\frac{1}{2},j,k-1} - u_{i-\frac{1}{2},j,k-1}}{2\delta z} .$$

The other derivatives $\left[\frac{\partial v}{\partial x}\right]_{i,j,k}$ and $\left[\frac{\partial w}{\partial x}\right]_{i,j,k}$ are obtained similarly.

Once $q_{i,j,k}$ has been calculated, the value of $\nu(q_{i,j,k})$ follows from (20).

Thus, $\widetilde{p}_{i,j,k}$ is approximated by (making using of (37))

$$\widetilde{p}_{i,j,k} = \frac{1}{Re}\nu(q_{i,j,k})\left[2\left(\frac{u_{i+\frac{1}{2},j,k}-u_{i-\frac{1}{2},j,k}}{\delta x}\right)+\left(\frac{u_{i+\frac{1}{2},j,k}+u_{i-\frac{1}{2},j,k}-u_{i+\frac{1}{2},j,k-1}-u_{i-\frac{1}{2},j,k-1}}{2\delta z}\right)\right.$$
$$\left.+\left(\frac{w_{i,j,k+\frac{1}{2}}+w_{i,j,k-\frac{1}{2}}-w_{i-1,j,k+\frac{1}{2}}-w_{i-1,j,k-\frac{1}{2}}}{2\delta x}\right)\right] .$$

Other configurations of surface cells having only two adjacent faces contiguous with two empty cell faces are treated similarly.

4.4.3 60^0–sloped planar surface: These surfaces are defined to have the local unit vector making $\mathbf{60^0}$ with the coordinate axes. They are identified by surface cells having three adjacent faces contiguous with empty cell faces (see figure 6b). For these surfaces the normal vector takes the form $\mathbf{n} = \left(\pm\frac{\sqrt{3}}{3}, \pm\frac{\sqrt{3}}{3}, \pm\frac{\sqrt{3}}{3}\right)$. It can be seen that there are 8 different configurations of these planar surfaces. The approximating equations for one particular case will be given here; for details of each case see Tomé et al. [20].

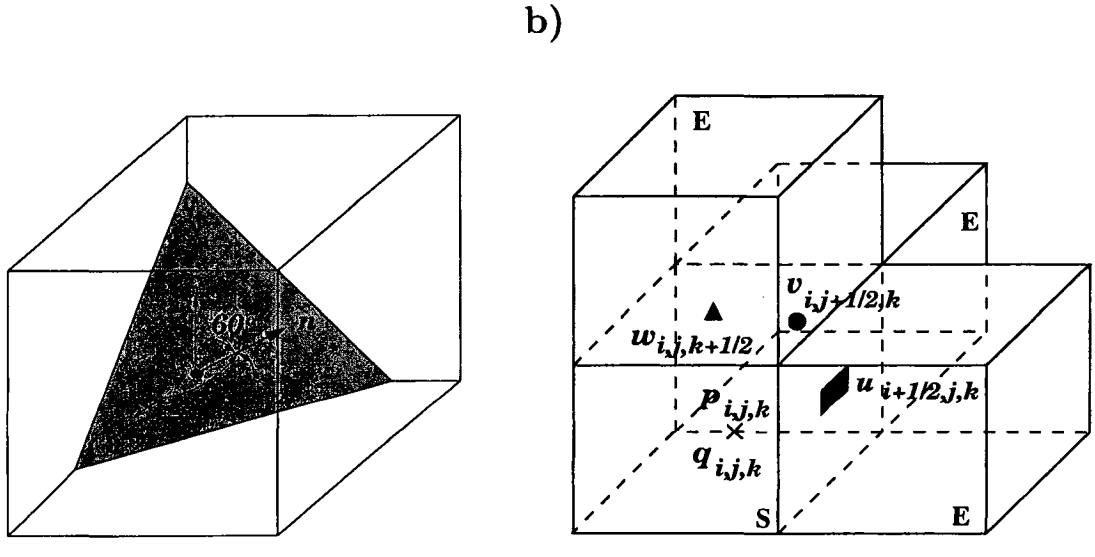

Fig. 6. An example of a $\mathbf{60^0}$–planar surface and a **S**–cell with the $(i+\frac{1}{2})$ and $(j+\frac{1}{2})$ and $(k+\frac{1}{2})$–faces contiguous with **E**–cell faces.

Let us consider the surface cell in figure 6b. For this cell we assume the local unit vectors take the form:

$$\mathbf{n} = \left(\frac{\sqrt{3}}{3}, \frac{\sqrt{3}}{3}, \frac{\sqrt{3}}{3}\right) , \quad \mathbf{m1} = \left(0, \frac{\sqrt{2}}{2}, -\frac{\sqrt{2}}{2}\right) , \quad \mathbf{m2} = \left(-2\frac{\sqrt{6}}{6}, \frac{\sqrt{6}}{6}, \frac{\sqrt{6}}{6}\right) .$$

Introducing **n**, **m1** and **m2** into (25)–(27) we obtain

$$p - \frac{2}{3Re}\nu(q)\left[\left(\frac{\partial u}{\partial y}+\frac{\partial v}{\partial x}\right)+\left(\frac{\partial u}{\partial z}+\frac{\partial w}{\partial x}\right)+\left(\frac{\partial v}{\partial z}+\frac{\partial w}{\partial y}\right)\right] = 0\,, \quad (39)$$

$$2\frac{\partial v}{\partial y}-2\frac{\partial w}{\partial z}+\left(\frac{\partial u}{\partial y}+\frac{\partial v}{\partial x}\right)-\left(\frac{\partial u}{\partial z}+\frac{\partial w}{\partial x}\right) = 0\,, \quad (40)$$

$$-4\frac{\partial u}{\partial x}+2\frac{\partial v}{\partial y}+2\frac{\partial w}{\partial z}-\left(\frac{\partial u}{\partial y}+\frac{\partial v}{\partial x}\right)-\left(\frac{\partial u}{\partial z}+\frac{\partial w}{\partial x}\right)+2\left(\frac{\partial v}{\partial z}+\frac{\partial w}{\partial y}\right) = 0\,, \quad (41)$$

respectively. Adding (40) and (41) yields

$$-4\frac{\partial u}{\partial x}+4\frac{\partial v}{\partial y}-2\left(\frac{\partial u}{\partial z}+\frac{\partial w}{\partial x}\right)+2\left(\frac{\partial v}{\partial z}+\frac{\partial w}{\partial y}\right)=0\,. \quad (42)$$

Mass conservation for these cells also requires

$$\frac{\partial u}{\partial x}+\frac{\partial v}{\partial y}+\frac{\partial w}{\partial z}=0\,. \quad (43)$$

The values of $u_{i+\frac{1}{2},j,k}$, $v_{i,j+\frac{1}{2},k}$ and $w_{i,j,k+\frac{1}{2}}$ are needed. They are obtained by applying (40), (42) and (43) at the surface cell centre. Once again details of the finite difference equations involved can be found in Tomé et al. [20]. Next we present the difference equations for calculating $q_{i,j,k}$ and the pressure at the surface cell centre.

Computation of $q_{i,j,k}$.

The value of $q_{i,j,k}$ is obtained by discretizing (19) at the centre of the surface cell. The derivatives $\left[\frac{\partial u}{\partial x}\right]_{i,j,k}$, $\left[\frac{\partial v}{\partial y}\right]_{i,j,k}$ and $\left[\frac{\partial w}{\partial z}\right]_{i,j,k}$ are approximated by central differences while the cross derivatives are obtained using forward and/or backward differences. For instance, for the surface cell shown in figure 8 we have

$$\begin{aligned}
q_{i,j,k} = \Bigg(& 2\left(\frac{u_{i+\frac{1}{2},j,k}-u_{i-\frac{1}{2},j,k}}{\delta x}\right)^2+2\left(\frac{v_{i,j+\frac{1}{2},k}-v_{i,j-\frac{1}{2},k}}{\delta y}\right)^2+2\left(\frac{w_{i,j,k+\frac{1}{2}}-w_{i,j,k-\frac{1}{2}}}{\delta z}\right)^2 \\
& +\left(\frac{u_{i+\frac{1}{2},j,k}+u_{i-\frac{1}{2},j,k}-u_{i+\frac{1}{2},j-1,k}-u_{i-\frac{1}{2},j-1,k}}{2\delta y}+\frac{v_{i,j+\frac{1}{2},k}+v_{i,j-\frac{1}{2},k}-v_{i-1,j+\frac{1}{2},k}-v_{i-1,j-\frac{1}{2},k}}{2\delta x}\right)^2 \\
& +\left(\frac{u_{i+\frac{1}{2},j,k}+u_{i-\frac{1}{2},j,k}-u_{i+\frac{1}{2},j,k-1}-u_{i-\frac{1}{2},j,k-1}}{2\delta z}+\frac{w_{i,j,k+\frac{1}{2}}+w_{i,j,k-\frac{1}{2}}-w_{i-1,j,k+\frac{1}{2}}-w_{i-1,j,k-\frac{1}{2}}}{2\delta x}\right)^2 \\
& +\left(\frac{v_{i,j+\frac{1}{2},k}+v_{i,j-\frac{1}{2},k}-v_{i,j+\frac{1}{2},k-1}-v_{i,j-\frac{1}{2},k-1}}{2\delta z}+\frac{w_{i,j,k+\frac{1}{2}}+w_{i,j,k-\frac{1}{2}}-w_{i,j-1,k+\frac{1}{2}}-w_{i,j-1,k-\frac{1}{2}}}{2\delta y}\right)^2\Bigg)^{\frac{1}{2}}\,.
\end{aligned}$$

Once the value of $q_{i,j,k}$ is computed, the viscosity follows from (20). Finally, the pressure follows from (40) applied at the surface cell centre, giving

$$\tilde{p}_{i,j,k} = \frac{2}{3Re}\nu(q_{i,j,k})\left[\left(\frac{u_{i+\frac{1}{2},j,k} + u_{i-\frac{1}{2},j,k} - u_{i+\frac{1}{2},j-1,k} - u_{i-\frac{1}{2},j-1,k}}{\delta y} + \frac{v_{i,j+\frac{1}{2},k} + v_{i,j-\frac{1}{2},k}}{\delta x}\right.\right.$$
$$\left.\left.\frac{-v_{i-1,j+\frac{1}{2},k} - v_{i-1,j-\frac{1}{2},k}}{\delta x}\right) + \left(\frac{u_{i+\frac{1}{2},j,k} + u_{i-\frac{1}{2},j,k} - u_{i+\frac{1}{2},j,k-1} + u_{i-\frac{1}{2},j,k-1}}{\delta z}\right.\right.$$
$$\left.\left.+ \frac{w_{i,j,k+\frac{1}{2}} + w_{i,j,k-\frac{1}{2}} - w_{i-1,j,k+\frac{1}{2}} - w_{i-1,j,k-\frac{1}{2}}}{\delta x}\right) + \left(\frac{v_{i,j+\frac{1}{2},k} + v_{i,j-\frac{1}{2},k}}{\delta z}\right.\right.$$
$$\left.\left.\frac{-v_{i,j+\frac{1}{2},k-1} - v_{i,j-\frac{1}{2},k-1}}{\delta z} + \frac{w_{i,j,k+\frac{1}{2}} + w_{i,j,k-\frac{1}{2}} - w_{i,j-1,k+\frac{1}{2}} - w_{i,j-1,k-\frac{1}{2}}}{\delta y}\right)\right] .$$

The remaining configurations of surface cells having only three adjacent faces contiguous with empty cells are treated similarly. For details of each case see Tomé et al. [19]

4.5 Time-step Control and Free Surface Movement

A procedure for calculating the time-step is employed. The time-step size is computed according to the following stability restrictions

$$\delta t < \frac{\delta x}{|u|}, \qquad \delta t < \frac{\delta y}{|v|}, \qquad \delta t < \frac{\delta z}{|w|}, \tag{44}$$

$$\delta t < \frac{\delta x^2 \delta y^2 \delta z^2}{\delta x^2 \delta y^2 + \delta x^2 \delta z^2 + \delta y^2 \delta z^2} \frac{Re}{2} \frac{1}{\nu_{max}}, \tag{45}$$

where ν_{max} is the maximum value of the viscosity within the bulk fluid. For the calculations in this paper it has been found to be convenient (and satisfactory) to choose $\nu_{max} = 1$. The implementation of this time-step procedure follows the same ideas of Tome and McKee [21].

4.6 Marker particles and fluid visualization

The fluid is represented by a B-Rep data structure (see Mäntylä, [12]). The fluid surface is defined by a piecewise linear surface composed of triangles and/or quadrilaterals containing marker particles on their vertices. The fluid surface is updated in three stages: firstly, the surface is moved to the new location according to the newly computed velocity field; in the second stage new particles are inserted if required; thirdly, particles are removed from cells which have accumulated too many. A fluid particle moves according to the equation

$$\frac{d\mathbf{x}_p}{dt} = \mathbf{u}_p ,$$

where $\mathbf{u}_p$ is the velocity of the particle at position $\mathbf{x_p}$ at time t_{n+1}. By using Euler's method, the particles are moved to the new position

$$\begin{aligned} x^{n+1} &= x^n + u_p \delta t, \\ y^{n+1} &= y^n + v_p \delta t, \\ z^{n+1} &= z^n + w_p \delta t, \end{aligned}$$

where x^n, y^n, z^n is the original position of particle p at time t_n. The particle velocities u_p, v_p, w_p are found by performing a tri-linear approximation using the eight nearest velocities.

Particle insertion and delection are described in detail in Castelo et al. [2]. The specific details of the fluid visualization such as rendering, toning, light reflection, etc, may also be found in this paper.

5. Validation results

The finite difference equations described in Section 4 were incorporated into the Freeflow-3D code (see Castelo et al. [2]) in order to simulate unsteady non-Newtonian free surface flow.

5.1 Fully developed pipe flow

We validate the numerical method presented in this paper by simulating an axisymmetric flow in a pipe. We consider a pipe of radius R and having a length of $L = 10R$ (see figure 7).

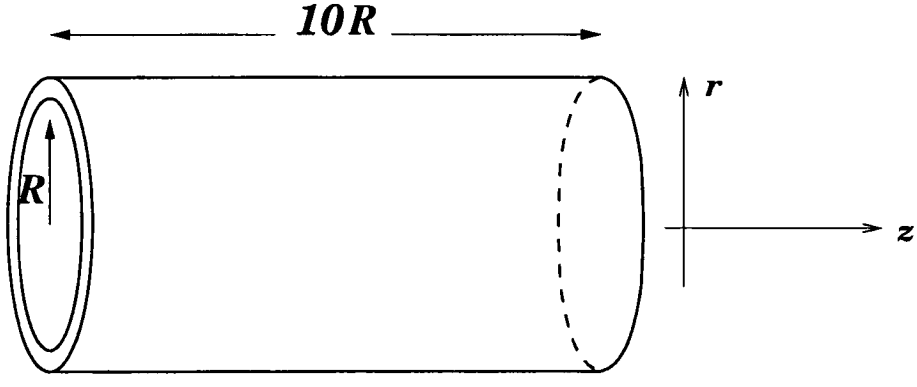

Fig. 7. Numerical simulation of a pipe flow: 3D case.

If we consider axisymmetric flow of a generalized fluid with $\mathbf{v} = (v_r, v_z)$, then the governing equations can be written as

$$\frac{\partial v_r}{\partial t} + \frac{1}{r}\frac{\partial (r v_r^2)}{\partial r} + \frac{\partial (v_r v_z)}{\partial z} = -\frac{\partial p}{\partial r} + \frac{\nu(q)}{Re}\frac{\partial}{\partial z}\left(\frac{\partial v_r}{\partial z} - \frac{\partial v_z}{\partial r}\right)$$
$$+\frac{1}{Re}\left[2\frac{\partial v_r}{\partial r}\frac{\partial \nu(q)}{\partial r} + \left(\frac{\partial v_r}{\partial z} + \frac{\partial v_z}{\partial r}\right)\frac{\partial \nu(q)}{\partial z}\right] + \frac{1}{Fr^2}g_r \ , \tag{46}$$

$$\frac{\partial v_z}{\partial t} + \frac{1}{r}\frac{\partial (r v_r v_z)}{\partial r} + \frac{\partial (v_z^2)}{\partial z} = -\frac{\partial p}{\partial z} - \frac{\nu(q)}{Re}\frac{1}{r}\frac{\partial}{\partial r}\left(r\left(\frac{\partial v_r}{\partial z} - \frac{\partial v_z}{\partial r}\right)\right)$$
$$+\frac{1}{Re}\left[2\frac{\partial v_z}{\partial z}\frac{\partial \nu(q)}{\partial z} + \left(\frac{\partial v_r}{\partial z} + \frac{\partial v_z}{\partial r}\right)\frac{\partial \nu(q)}{\partial r}\right] + \frac{1}{Fr^2}g_z \ , \tag{47}$$

$$\frac{1}{r}\frac{\partial (r v_r)}{\partial r} + \frac{\partial v_z}{\partial z} = 0 \ , \tag{48}$$

where v_r and v_z are the velocity components in the r and z- directions respectively. By assuming fully developed flow, equations (46) – (48) reduce to

$$\frac{\partial}{\partial r}\left(\nu(q)\frac{\partial v_z}{\partial r}\right) + \frac{1}{r}\nu(q)\frac{\partial v_z}{\partial r} = Re\frac{\partial p}{\partial z} \tag{49}$$

where $q = |\frac{\partial v_z}{\partial r}|$ is the shear rate. Equation (49) is solved subject to the boundary conditions

$$\frac{\partial v_z}{\partial r}|_{r=0} = 0 \ , \qquad v_z|_{r=R} = 0 \ . \tag{50}$$

The boundary value problem defined by (49)-(50) is solved as follows. Firstly, we rewrite (49) as the initial value problem

$$\frac{\partial Z}{\partial r} + \frac{Z}{r} = \alpha \ , \quad Z(0) = 0 \tag{51}$$

where $Z = \nu(q)\frac{\partial v_z}{\partial r}$ and $\alpha = Re\frac{\partial p}{\partial z}$. The solution of this initial value problem is $Z(r) = \frac{1}{2}\alpha r$, namely

$$\nu(q)\frac{\partial v_z}{\partial r} = \frac{1}{2}\alpha r \ . \tag{52}$$

Now, if we use the Cross model, equation (52) becomes

$$\left(\nu_\infty + \frac{\nu_0 - \nu_\infty}{1 + (Kq)^m}\right)\frac{\partial v_z}{\partial r} = \frac{1}{2}\alpha r. \tag{53}$$

If we consider a steady flow in a pipe then due to symmetry we can assume $q = \left|\frac{\partial v_z}{\partial r}\right| = \frac{\partial v_z}{\partial r} > 0$. Equation (53) can be written in form

$$\nu_\infty K^m \left(\frac{\partial v_z}{\partial r}\right)^{m+1} - \frac{1}{2}\alpha K^m r \left(\frac{\partial v_z}{\partial r}\right)^m + \nu_0 \frac{\partial v_z}{\partial r} - \frac{1}{2}\alpha r = 0 \ . \tag{54}$$

By taking $m = 1$, equation (54) becomes

$$\nu_\infty K \left(\frac{\partial v_z}{\partial r}\right)^2 + (\nu_0 - \frac{1}{2}\alpha K r)\left(\frac{\partial v_z}{\partial r}\right) - \frac{1}{2}\alpha r = 0 \tag{55}$$

which gives

$$\left(\frac{\partial v_z}{\partial r}\right) = \frac{-(\nu_0 - \frac{1}{2}\alpha K r) \pm \sqrt{(\nu_0 - \frac{1}{2}\alpha K r)^2 + 2\nu_\infty \alpha K r}}{2\nu_\infty K} \ . \tag{56}$$

Integrating (56) over $[r,\ R]$ we have

$$v_z(r) = v_z(R) - \frac{1}{2\nu_\infty K}\left[-\nu_0(R-r) + \frac{1}{4}K\alpha(R^2 - r^2) \pm \int_r^R \sqrt{(\nu_0 - \frac{1}{2}\alpha K s)^2 + 2\nu_\infty \alpha K s}\ ds\right] \tag{57}$$

After solving the integral in (57) (see [8], page 81) we obtain (since $v_z(R) = 0$)

$$\begin{aligned} v_z(r) = -\frac{1}{2\nu_\infty K}\Bigg\{-\nu_0(R-r) + \frac{1}{4}K\alpha(R^2 - r^2) \pm \Bigg[\frac{2cR+b}{4c}\sqrt{cR^2 + bR + a} \\ -\frac{2cr+b}{4c}\sqrt{cr^2 + br + a} + \frac{\Delta}{8c}\frac{1}{\sqrt{c}}\left(\operatorname{arcsinh}\left(\frac{2cR+b}{\sqrt{\Delta}}\right) - \operatorname{arcsinh}\left(\frac{2cr+b}{\sqrt{\Delta}}\right)\right)\Bigg]\Bigg\} \end{aligned} \tag{58}$$

where

$$c = \frac{1}{4}(K\alpha)^2 \ , \quad b = K\alpha(2\nu_\infty - \nu_0) \ , \quad a = \nu_0^2 \ , \quad \Delta = 4ac - b^2 = 4K^2\alpha^2\nu_\infty(\nu_0 - \nu_\infty) \ .$$

Equation (58) gives two solutions but only one of them satisfies the boundary condition $\frac{\partial v_z}{\partial r}|_{r=0} = 0$.

To validate the numerical method presented in this paper we simulated the flow in a pipe and made a comparison with the analytical solution given by (58). We considered the pipe as shown in figure 7. The fluid is described by the Cross model with the parameters given by $\nu_0 = 0.2\text{m}^2\text{s}^{-1}, \nu_\infty = 0.02\text{m}^2\text{s}^{-1}, K = 2.0$ and $m = 1$. A mesh size of $\delta x = \delta y = \delta z = 0.1$ was employed and gravity was neglected. We first set $R = \nu_0 = 1$ and compute the velocity at the fluid entrance, U, at $t = 0$ from

$$U = \frac{1}{\pi R^2} \int_0^{2\pi} \int_0^R v_z(r) r dr d\theta \, . \tag{59}$$

The parameter α appearing in the $v_z(r)$ was set to $\alpha = 0.357258$ giving the velocity at the inlet, as calculated using (59) to be $U = 1\text{ms}^{-1}$. We ran the Freeflow-3D code with the data above. We started with an empty pipe and injected fluid at the inlet until the pipe was full and the steady state was reached. Figure 8 displays the fluid flow configuration at different times. Figure 9 shows the variation of the velocity w and the viscosity at the cross-section of the pipe situated at the position $z = 7.5$. Figure 10 displays the numerical and the analytical values of the axial velocity at the cross-section of the pipe at the position $z = 7.5$. We see that the agreement between the two solutions is good.

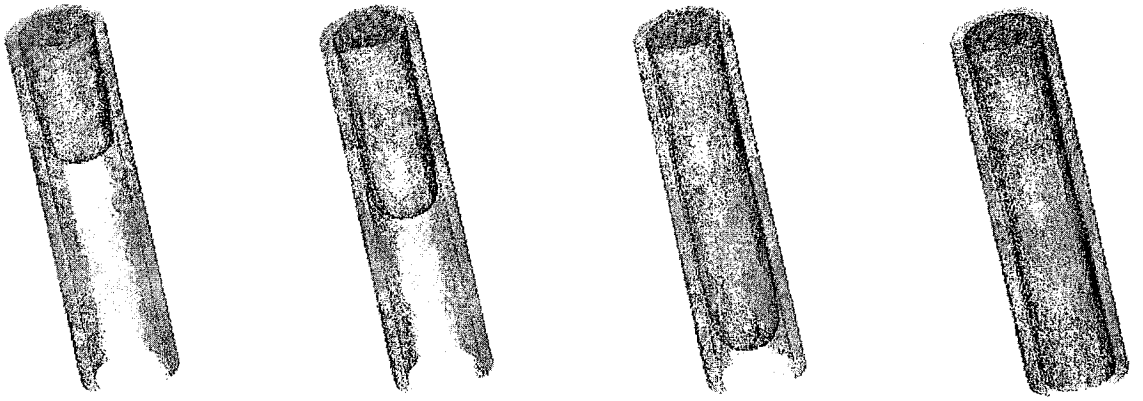

Fig. 8. Fluid flow configuration computed at different times: a) $t = 3.0$, b) $t = 4.5$, c) $t = 8.0$ and d) $t = 20$.

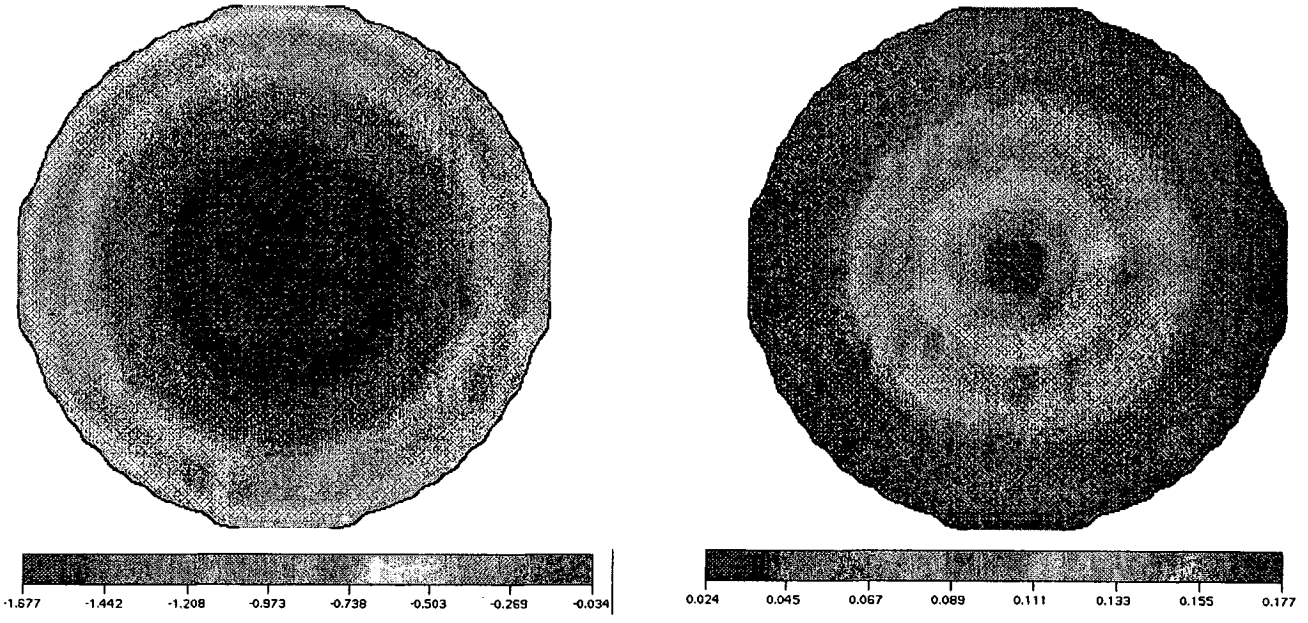

Fig. 9. Variation of the w-velocity and the viscosity computed at the cross section of the pipe $z = 7.5$ at time t = 20.

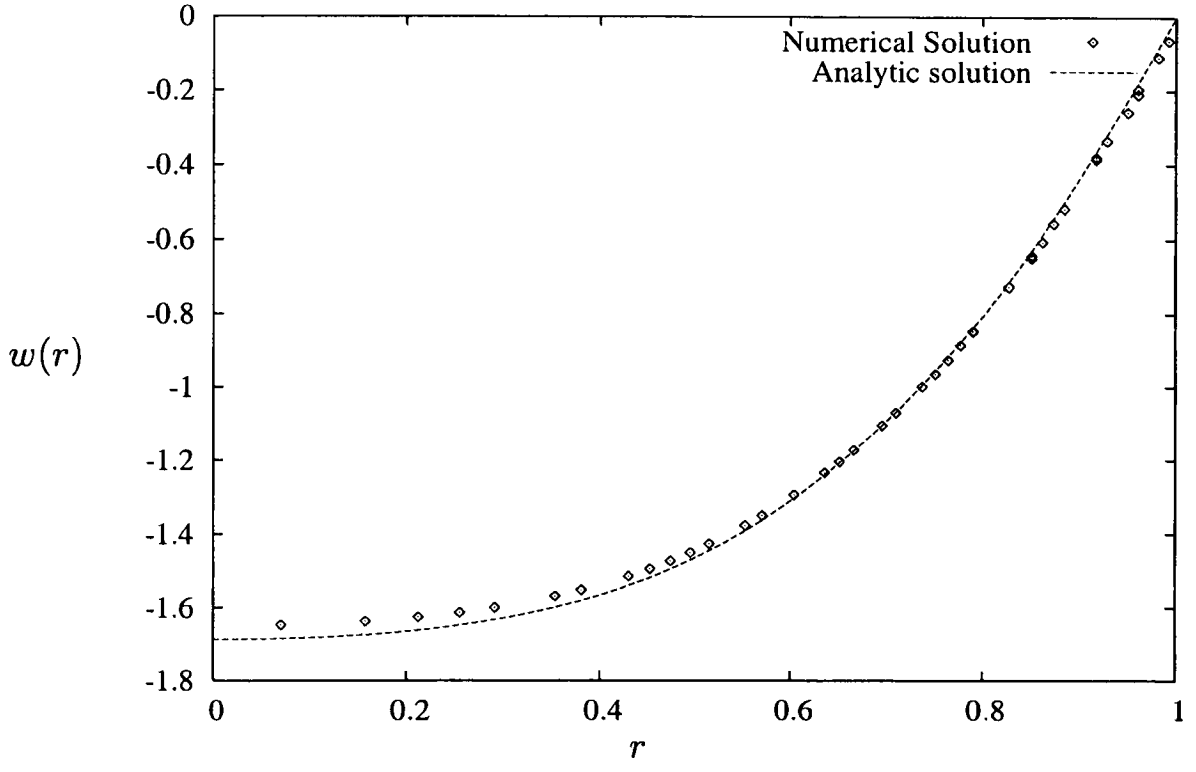

Fig. 10. Numerical simulation of pipe flow: comparison between analytical and numerical results at the cross-section of the pipe at $z = 7.5$. Time shown is $t = 20$.

To further verify the correctness of the code we performed an additional run and compared the numerical results with its corresponding analytic solution. We make $\nu_\infty = 0$ and $m = 1/2$ in equation (54) to obtain

$$-\frac{1}{2}\alpha K^{1/2} r \left(\frac{\partial v_z}{\partial r}\right)^{1/2} + \nu_0 \left(\frac{\partial v_z}{\partial r}\right) - \frac{1}{2}\alpha r = 0 \; . \tag{60}$$

By making the change of variables

$$\left(\frac{\partial v_z}{\partial r}\right) = \chi^2 \tag{61}$$

equation (60) becomes

$$-\frac{1}{2}\alpha K^{1/2} r \chi + \nu_0 \chi^2 - \frac{1}{2}\alpha r = 0 \; , \tag{62}$$

and solving for χ we obtain

$$\chi = \frac{1}{2\nu_0}\left[\frac{1}{2}\alpha K^{1/2} r \pm \sqrt{\frac{1}{4}\alpha^2 K r^2 + 2\nu_0 \alpha r}\right] \; . \tag{63}$$

Thus,

$$\left(\frac{\partial v_z}{\partial r}\right) = \frac{1}{4\nu_0^2}\left[\frac{1}{2}\alpha^2 K r^2 + 2\nu_0 \alpha r \pm \alpha K^{1/2} r \sqrt{\frac{1}{4}\alpha^2 K r^2 + 2\nu_0 \alpha r}\right] \; . \tag{64}$$

Integrating (64) over $[r,\ R]$ we obtain (since $v_z(R) = 0$)

$$v_z(r) = -\frac{1}{4\nu_0^2}\left[\frac{1}{6}\alpha^2 K(R^3 - r^3) + \nu_0\alpha(R^2 - r^2) \pm \frac{1}{2}\alpha K^{1/2}\int_r^R s\sqrt{\alpha^2 K s^2 + 8\nu_0\alpha s}\, ds\right] . \quad (65)$$

Solving the integral above (see [8], page 82) yields

$$\begin{aligned} v_z(r) = &-\frac{1}{4\nu_0^2}\left\{\frac{1}{6}\alpha^2 K(R^3 - r^3) + \nu_0\alpha(R^2 - r^2)\right. \\ &\pm\frac{1}{2}\alpha K^{1/2}\left[\frac{1}{3c}\left((S(R))^{3/2} - (S(r))^{3/2}\right) - \frac{1}{8c^2}\left((2cR+b)bS(R)^{1/2} - (2cr+b)bS(r)^{1/2}\right)\right. \\ &\left.\left.-\frac{b\Delta}{16c^2\sqrt{c}}\left(\ln\left(2\sqrt{c(S(R))} + 2cR + b\right) - \ln\left(2\sqrt{c(S(r))} + 2cr + b\right)\right)\right]\right\} , \end{aligned} \quad (66)$$

where

$$S(R) = \alpha^2 K R^2 + 8\nu_0\alpha R\ ,\ S(r) = \alpha^2 K r^2 + 8\nu_0\alpha r\ ,\ b = 8\nu_0\alpha\ ,\ c = \alpha^2 K \text{ and } \Delta = -64\nu_0^2\alpha^2$$

Again, we used the input data employed for the simulation of the flow in a pipe (see figure 7). For the Cross model we employed $K = 5.0$ and $\nu_0 = 0.20\text{m}^2\text{s}^{-1}$ and the parameter α appearing in the analytic solution (66) was set to $\alpha = 0.350$ and R was set to $R = 1$. The velocity at the pipe entrance was computed from (59) which gave the value of $U = 1.161\text{ms}^{-1}$. Thus, $Re = RU/\nu_0 = 5.805$ and $Fr = 2.698$. We run the Freeflow-3D code to simulate this pipe flow. Again, we started with the pipe empty and injected fluid at the inlet until the pipe was filled and steady state had been reached. The numerical results of this simulation together with the analytic solution at the cross section of the pipe situated at the position $z = 7.5$ are plotted in figure 11. As we can see from figure 11, the agreement between the numerical and the analytic results is good; this provides further validation for the methodology employed in this paper for solving the governing equations.

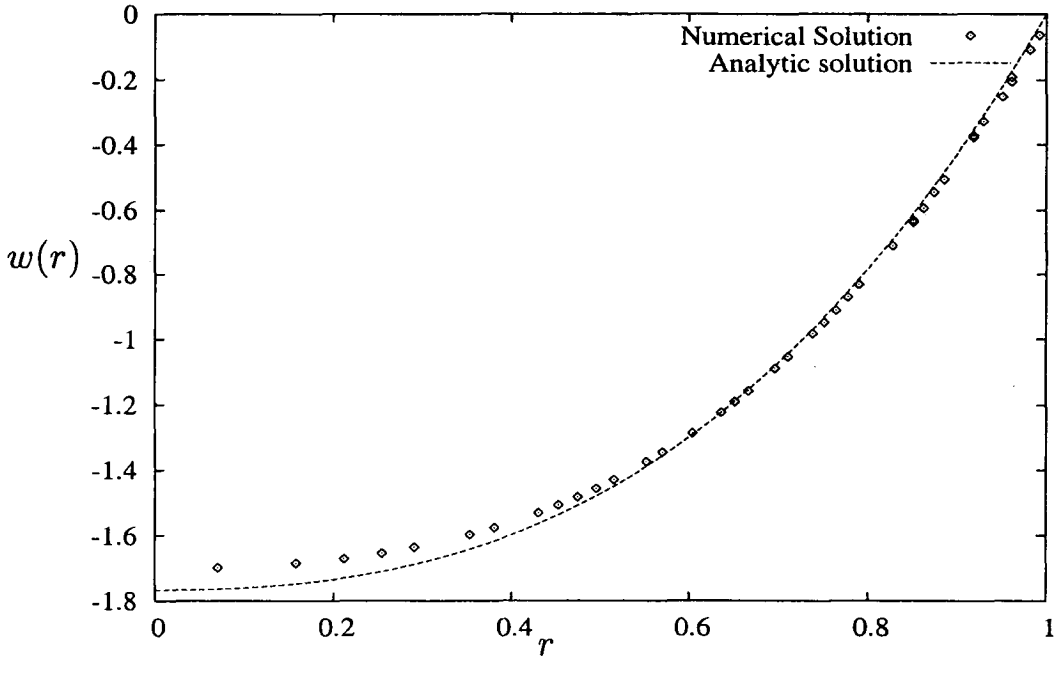

Fig. 11. Numerical simulation of pipe flow: comparison between analytical and the numerical results at the cross-section of the pipe at $z = 7.5$. Time shown is $t = 20$.

5.2. Numerical Simulation of non-Newtonian fluid flow instability

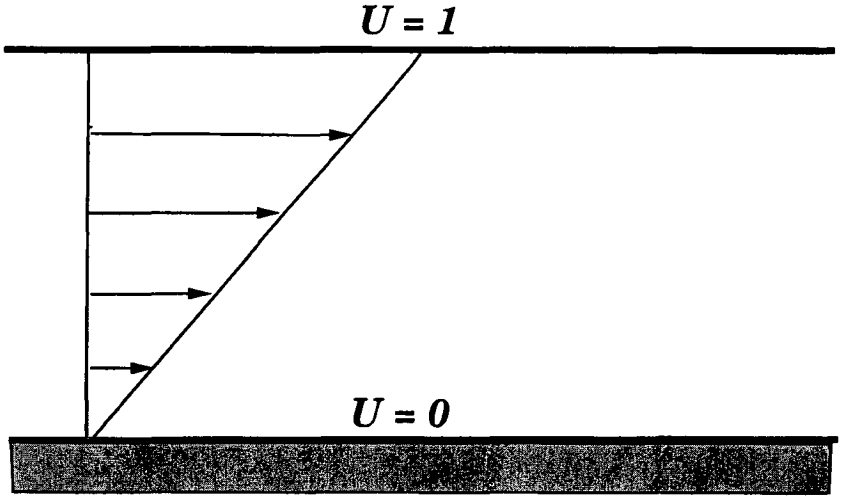

Fig. 12. Couette flow specification.

In generalized Newtonian fluids the equations become ill-posed on the decreasing branch of the shear stress-shear rate curve (see Renardy [14]). To show this, consider the flow between two parallel plates as shown in figure 12. For the case of one-dimensional flow the governing equation is (if we neglect body forces)

$$\frac{\partial u}{\partial t} = \frac{1}{Re}\left[\nu(q)\frac{\partial^2 u}{\partial y^2} + \frac{\partial u}{\partial y}\frac{\partial \nu}{\partial y}\right]. \tag{67}$$

In the case of steady state ($\frac{\partial u}{\partial t} = 0$), the solution $\bar{u}$ of this equation satisfies

$$\frac{1}{Re}\left[\nu(q)\frac{\partial^2 \bar{u}}{\partial y^2} + \frac{\partial \bar{u}}{\partial y}\frac{\partial \nu}{\partial q}\frac{\partial^2 \bar{u}}{\partial y^2}\right] = 0 \quad \Longrightarrow \quad \frac{1}{Re}\left[\nu(q) + \frac{\partial \bar{u}}{\partial y}\frac{\partial \nu}{\partial q}\right]\frac{\partial^2 \bar{u}}{\partial y^2} = 0. \tag{68}$$

Eq. (68) possesses two solutions, namely:

$$I) \quad \frac{\partial^2 \bar{u}}{\partial y^2} = 0 \qquad \text{and} \qquad II) \quad \frac{\partial \bar{u}}{\partial y} = -\frac{\nu(q)}{\dfrac{\partial \nu}{\partial q}}.$$

To analyse small pertubations about the steady state solution $\bar{u}$ of I), namely, $u = \bar{u} + \widehat{u}$ where $\widehat{u}$ is an infinitesimal pertubation we introduce u into (67), obtaining

$$\frac{\partial \widehat{u}}{\partial t} + \frac{\partial \bar{u}}{\partial t} = \frac{1}{Re}\left[\nu(q)\left(\frac{\partial^2 \bar{u}}{\partial y^2} + \frac{\partial^2 \widehat{u}}{\partial y^2}\right) + \left(\frac{\partial \bar{u}}{\partial y} + \frac{\partial \widehat{u}}{\partial y}\right)\frac{\partial \nu(q)}{\partial y}\right],$$

which simplifies to (since $\frac{\partial^2 \bar{u}}{\partial y^2} = 0$ and $\frac{\partial \bar{u}}{\partial t} = 0$)

$$\frac{\partial \widehat{u}}{\partial t} = \frac{1}{Re}\left[\nu(q)\frac{\partial^2 \widehat{u}}{\partial y^2} + \left(\frac{\partial \bar{u}}{\partial y} + \frac{\partial \widehat{u}}{\partial y}\right)\frac{\partial \nu(q)}{\partial y}\right]. \tag{70}$$

where $q = \bar{q} + \widehat{q} = |\frac{\partial \bar{u}}{\partial y} + \frac{\partial \widehat{u}}{\partial y}| = \frac{\partial \bar{u}}{\partial y} + \frac{\partial \widehat{u}}{\partial y}$, assuming that $\frac{\partial \bar{u}}{\partial y} > 0$ and $\frac{\partial \widehat{u}}{\partial y} << \frac{\partial \bar{u}}{\partial y}$.
If we neglect third and higher order terms, then the values of $\nu(q)$ and $\frac{\partial \nu(q)}{\partial y}$ can be obtained as follows:

$$\nu(q) \approx \nu(\bar{q}) + \left.\frac{\partial \nu(q)}{\partial q}\right|_{\bar{q}} \widehat{q} + \left.\frac{\partial^2 \nu(q)}{\partial q^2}\right|_{\bar{q}} \frac{\widehat{q}^2}{2!} , \tag{71}$$

which gives

$$\frac{\partial \nu(q)}{\partial q} \approx \left.\frac{\partial \nu(q)}{\partial q}\right|_{\bar{q}} + \left.\frac{\partial^2 \nu(q)}{\partial q^2}\right|_{\bar{q}} \widehat{q} .$$

Thus,

$$\begin{aligned} \frac{\partial \nu(q)}{\partial y} &= \frac{\partial \nu(q)}{\partial q}\frac{\partial q}{\partial y} \approx \left(\left.\frac{\partial \nu(q)}{\partial q}\right|_{\bar{q}} + \left.\frac{\partial^2 \nu(q)}{\partial q^2}\right|_{\bar{q}} \widehat{q} \right) \left(\frac{\partial \bar{q}}{\partial y} + \frac{\partial \widehat{q}}{\partial y} \right) \\ &= \left(\left.\frac{\partial \nu(q)}{\partial q}\right|_{\bar{q}} + \left.\frac{\partial^2 \nu(q)}{\partial q^2}\right|_{\bar{q}} \widehat{q} \right) \left(\frac{\partial^2 \bar{u}}{\partial y^2} + \frac{\partial^2 \widehat{u}}{\partial y^2} \right) . \end{aligned} \tag{73}$$

Again, neglecting second and higher order terms, we have

$$\frac{\partial \nu(q)}{\partial y} = \left.\frac{\partial \nu(q)}{\partial q}\right|_{\bar{q}} \frac{\partial^2 \widehat{u}}{\partial y^2} . \tag{74}$$

Introducing (71) and (74) into (70) we obtain

$$\frac{\partial \widehat{u}}{\partial t} = \frac{1}{Re} \left[\left(\nu(\bar{q}) + \left.\frac{\partial \nu(q)}{\partial q}\right|_{\bar{q}} \widehat{q} + \left.\frac{\partial^2 \nu(q)}{\partial q^2}\right|_{\bar{q}} \frac{\widehat{q}}{2} \right) \frac{\partial^2 \widehat{u}}{\partial y^2} + \left(\frac{\partial \bar{u}}{\partial y} + \frac{\partial \widehat{u}}{\partial y} \right) \left.\frac{\partial \nu(q)}{\partial q}\right|_{\bar{q}} \frac{\partial^2 \widehat{u}}{\partial y^2} \right] ,$$

which simplifies to (since $\widehat{u}$ is an infinitesimal pertubation)

$$\frac{\partial \widehat{u}}{\partial t} = \frac{1}{Re} \left[\nu(\bar{q}) + \bar{q} \left.\frac{\partial \nu(q)}{\partial q}\right|_{\bar{q}} \right] \frac{\partial^2 \widehat{u}}{\partial y^2} . \tag{76}$$

Equation (76) ceases to be parabolic when $\nu(\bar{q}) + \bar{q} \left.\frac{\partial \nu(q)}{\partial q}\right|_{\bar{q}}$ becomes negative. Thus, the flow will become unstable in regions of simple shear where

$$\gamma(q) = \frac{q}{\nu(q)} \frac{\partial \nu(q)}{\partial q} < -1 .$$

Figure 13 displays the left hand side of this equation for selected values of the parameters of the Cross model. We see that for the case of $m = 1.4$ and $m = 1.8$ there is instability for a certain range of the q.

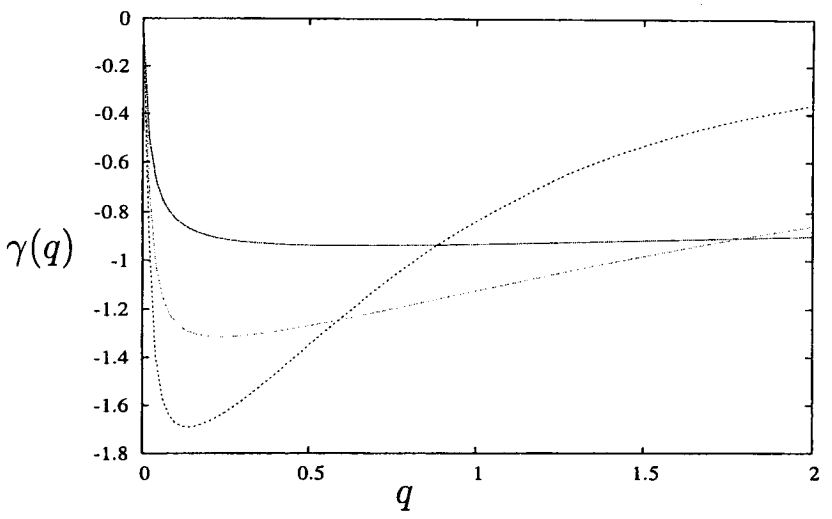

Fig. 13. $\gamma(q)$ variation as a function of the parameter m. Cross model parameters: $\nu_0 = 0.02\text{m}^2\text{s}^{-1}, \nu_\infty = 0.001\text{m}^2\text{s}^{-1}, K = 1$. Scaling parameters employed: $U = 0.5$, $L = 0.01$ and ν_0.

When the Cross model parameters are such that $\gamma(q) < -1$ for some range of q, the problem is ill-posed, and therefore unstable in regions of the flow where the shear rate is in this range. Although this analysis is for Couette flow, numerical simulations suggest that it is valid more generally. Indeed figure 14 displays a jet attempting to impinge on a flat plate. In this case the flow starts to develop instabilities even before it reaches the lower plate, and the solution becomes unphysical.

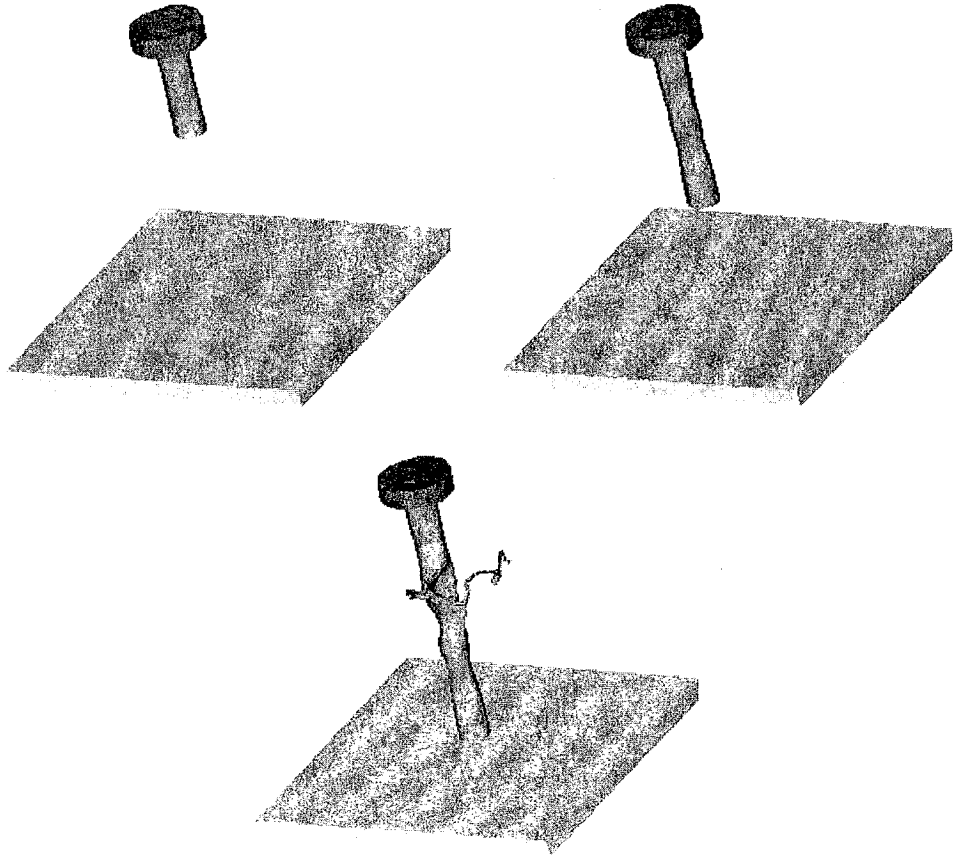

Fig. 14. Numerical simulation of fluid flow instability due to the Cross model. Cross model parameters are: $\nu_0 = 0.02\text{m}^2\text{s}^{-1}, \nu_\infty = 0.001\text{m}^2\text{s}^{-1}, K = 1$ and $m = 1.8$. In this case $\gamma(q)$ lies in the range $[0, -1.7]$ (see figure 13).

6. Numerical Results

In this section we present some calculational examples of free surface flows of generalized Newtonian fluids. Three rather different flow situations are presented; all of them display shear-thinning.

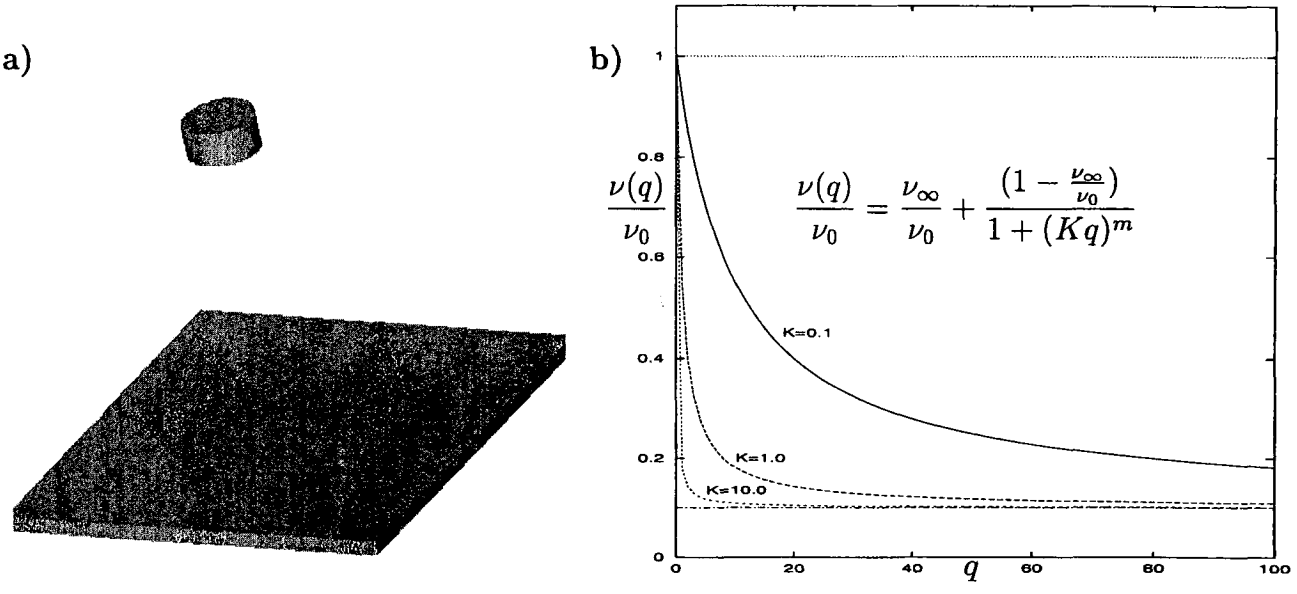

Fig. 15. Problem specification and viscosity variation as a function of the parameter K.

6.1 Simulation of a jet impinging onto a flat surface

We consider a flat surface and an axisymmetric jet issuing from an axisymmetric nozzle onto the flat surface at a prescribed velocity (see figure 15a). The following input data were employed: domain dimensions: 8cm × 8cm × 7cm; mesh size: 80 × 80 × 70 cells ($\delta x = \delta y = \delta z = 1$mm); jet diameter ($D$): 8mm; fluid velocity at the nozzle) (U): 0.25ms^{-1} ; flat surface dimensions: 8cm ×8cm with wall thickness 3mm; nozzle dimensions: 8mm diameter and 7mm height; height of nozzle (H): 6cm (distance of the nozzle to the flat surface); convergence criteria for the Poisson equation: EPS = 10^{-7} ; gravity was taken to act in the negative $z-$direction with $g_z = -9.81\text{ms}^{-2}$. The fluid was modelled by the Cross model using $\nu_0 = 0.002\text{m}^2\text{s}^{-1}$, $\nu_\infty = 0.0002\text{m}^2\text{s}^{-1}$ and $m = 1$. The scaling parameters used were U, D and ν_0 so that $Re = UD/\nu_0 = 1.0$ and $Fr = 0.8924$. The no-slip condition was applied on the flat surface.

Figure 16 displays three-dimensional flow visualizations at times $t = 0.15$s, $t = 0.30$s and $t = 0.70$s. The first column is simply Newtonian flow with $\nu = \nu_0$ ($Re = 1$); the second, the third and the fourth column displays non-Newtonian flow using the Cross model with $m = 1$ and K equal to 0.1, 1.0 and 10 respectively. Finally, the last column is again Newtonian flow with $\nu = \nu_\infty$ ($Re = 10$). Thus, all five flows are fairly viscous although we may note that as K increases the flows do become less viscous and consequently spread out further; this is particularly noticeable in figure 16. Clearly the greatest rate of shear will occur as the jet impinges on the flat surface where the fluid most abruptly changes direction and flows radially. In a shear-thinning fluid this has the effect of lowering the viscosity locally allowing the fluid

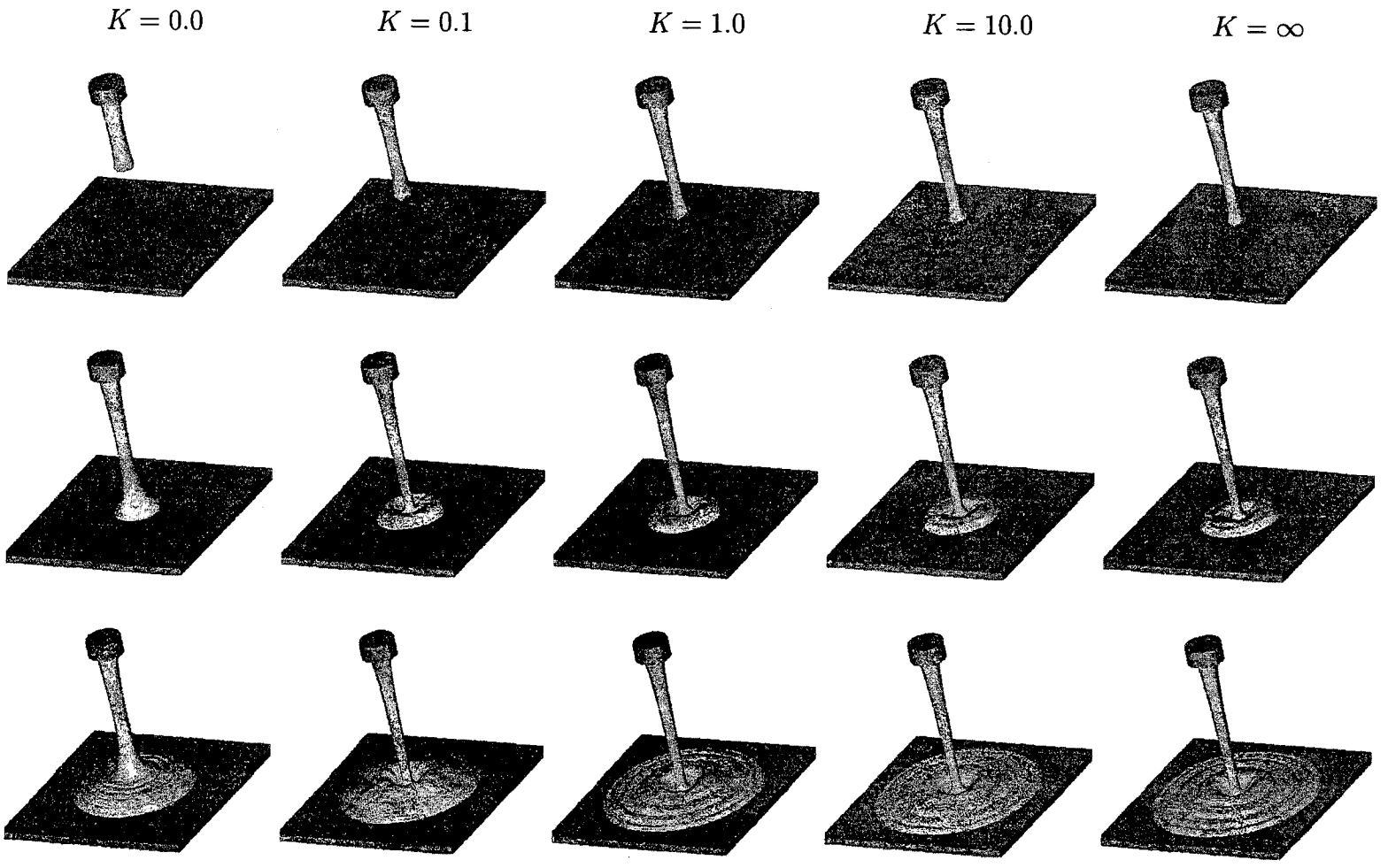

Fig. 16. Numerical simulation of a non-Newtonian jet impinging onto a flat surface at times $t = 0.15$s (top row), 0.30s (middle row) and $t = 0.70$s (bottom row). Three-dimensional view.

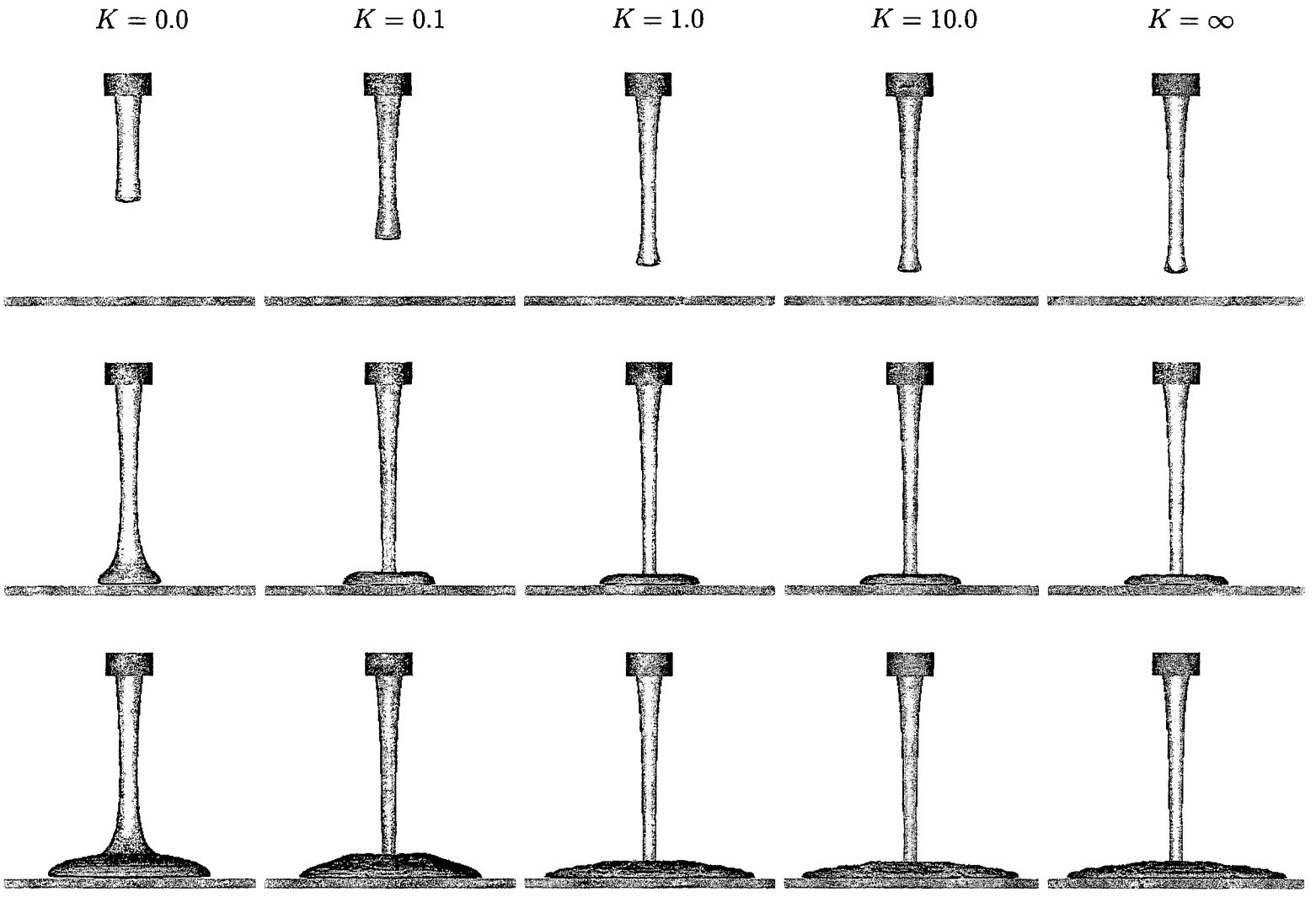

Fig. 17. Numerical simulation of a non-Newtonian jet impinging onto a flat surface at times $t = 0.15$s (top row), 0.30s (middle row) and $t = 0.70$s (bottom row). Frontal view.

to move more freely and rapidly. This is dramatically demonstrated when we compare the first column ($K = 0$) with the second column ($K = 0.1$): the local lowering of the viscosity about the point of impingement causes a pronounced indenture where the rate of shear is high. Of course the actual distance traversed by the fluid is only marginally greater in the case $K = 0.1$. This is because the rate of shear ceases to be large after the fluid emerges from the indenture and the local viscosity reverts to a value near ν_0. Two other features may be observed from figures 16 and 17: in the Newtonian case ($K = 0$) the viscous jet undergoes thickening near the base; and in all five cases surface waves or ripples may be observed. Both of these phenomena are simply due to the fact that we are dealing with a viscous fluid that is unable to remove itself sufficiently quickly before the fluid behind catches up.

6.2 Numerical Simulation of Jet Buckling

When a low Reynolds number jet flows onto a rigid plate, a phenomenon known as jet buckling can occur if the Reynolds number is smaller than a prescribed value. This phenomenon has attracted a number of investigators and it has been studied both experimentally and numerically. Cruickshank and Munson [6] and Cruickshank [5] have presented both experimental and theoretical results for Newtonian jets. From their study they obtained estimates for when jet buckling might occur: these are based upon the Reynolds number and the ratio H/D (H is the height of the inlet to the rigid plate and D is the jet diamenter). In particular, they found that a two-dimensional jet will buckle if the following conditions

$$Re < 0.5 \qquad \text{and} \qquad H/D > 10$$

are satisfied. For an axisymmetric jet they found that the buckling conditions were modified to

$$Re < 1.2 \qquad \text{and} \qquad H/D > 7\ . \tag{78}$$

Numerically, this problem has been investigated by Tomé and McKee [22] who performed a numerical study of two-dimensional jet buckling; three-dimensional jet buckling has been simulated by Castelo et al. [2] for 3D- Newtonian flows using square cross sectional jets; and Tomé et al. [23] have studied two-dimensional viscoelastic jets.

To demonstrate that the finite difference method presented in this paper can deal with shear thining fluids, we present in this section two calculations that simulate the buckling of an axisymmetric viscous jet hitting a rigid plate. For a Newtonian jet the Reynolds number is a dominant factor indicating the behaviour of the flow, whereas for a generalized Newtonian jet the "Reynolds number" is varying locally according to the shear rate. To illustrate that the variation of the viscosity with the shear rate has a strong effect on the buckling phenomenon, we present two calculations that constrast Newtonian with non-Newtonian behaviour; in both cases Cruickshank's conditions (78) are satisfied, predicting buckling of the Newtonian jet. The first calculation concerns a thin jet of diameter of $D = 5$ mm issued from an inlet situated at a height $H = 5$cm above the plate (so that $H/D = 10$) and flowing onto a rigid plate of dimensions 5cm $\times$ 5cm $\times$ 3mm (see figure 15a for details). A uniform input velocity of $U = 1\text{ms}^{-1}$ was set at the inlet and the fluid were modelled by the Cross model with associated parameters chosen to be

$$\nu_\infty = 0.02\text{m}^2\text{s}^{-1}\ , \quad \nu_0 = 0.002\text{m}^2\text{s}^{-1}\ , \quad m = 0.5 \quad K = 0.1\ .$$

The scaling paramenters U, D, ν_0 were chosen so that $Re = 0.25$ and $1/F_r^2 = 0.049$. Figure 18 displays a comparison between the Newtonian ($K = 0$) and the non-Newtonian three-dimensional fluid flow configurations at different times.

The second calculation also concerns a thin jet flowing down to a rigid plate. The fluid properties were chosen to be

$$\nu_\infty = 0.005\text{m}^2\text{s}^{-1} \ , \quad \nu_0 = 0.0005\text{m}^2\text{s}^{-1} \ , \quad m = 0.5 \quad K = 0.1 \ .$$

The inlet diameter is $D = 6$mm and the inlet velocity is $U = 0.5\text{ms}^{-1}$. This gives $Re = UD/\nu_0 = 0.6$ and $1/F_r^2 = 0.2354$ and a slenderness ratio of $H/D = 8.3$. Again, Cruickshank's analysis predicts that the Newtonian jet will buckle. Our results are displayed in figures 18 and 19.

We can observe in figure 18 that the Newtonian jet has already buckled at $t = 0.1875$s while the generalized Newtonian jet has undergone only small asymmetry at that time, indicating the onset of buckling. By the time $t = 0.375$s there are many folds in the Newtonian fluid and the phenomenon known as 'coiling' (see Cruickshank [5]) has taken place. In the generalized Newtonian fluid coiling is less pronounced.

In figure 19 the differences are even more dramatic: the Newtonian jet becomes thicker on hitting the rigid plate and then at time $t = 0.25$s it buckles whereas the generalized Newtonian jet does not become noticeably thicker but flows radially without any evidence of buckling. Indeed, as the flow is hindered by the no-slip condition on the rigid plate, the Newtonian fluid accumulates, and by obstructing the oncoming fluid initiates buckling. In the generalized Newtonian case, the higher shear rates near the rigid plate lead to a lower viscosity and therefore to a greater mobility. This allows the fluid to flow radially so that there is no obstruction to oncoming fluid and buckling does not occur: an effective Reynolds number Re^* in the generalized Newtonian case is higher due to the decreased viscosity, presumably taking Re^* beyond Cruickshank's critical value of 1.2. This result was also observed by Tome et al. ([18]) for the two-dimensional case.

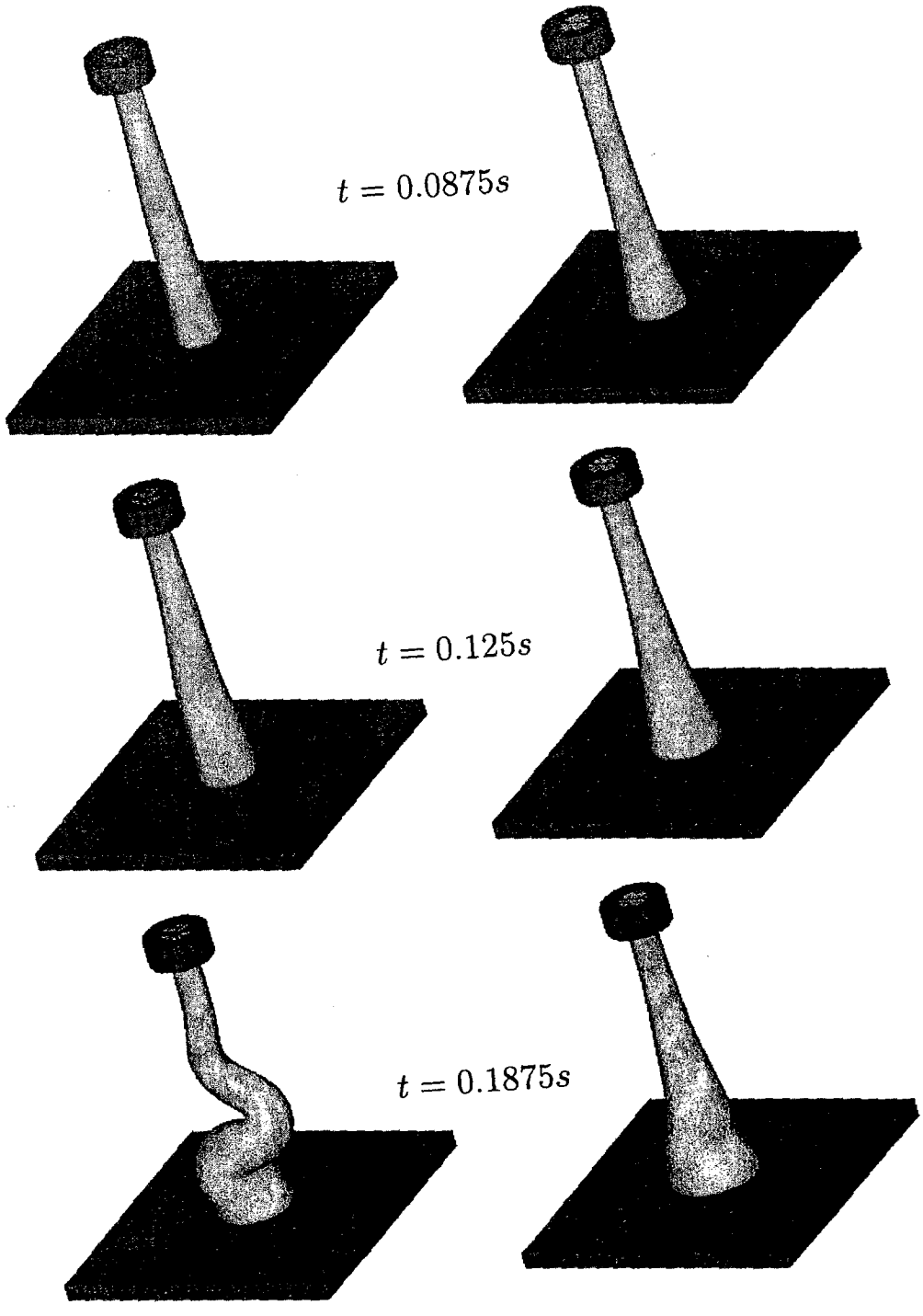

Fig. 18. Numerical simulation of three-dimensional jet buckling. Newtonian jet (on the left) and non-Newtonian jet (on the right). Fluid flow visualization at different times - 3D-view. $Re = 0.25$.

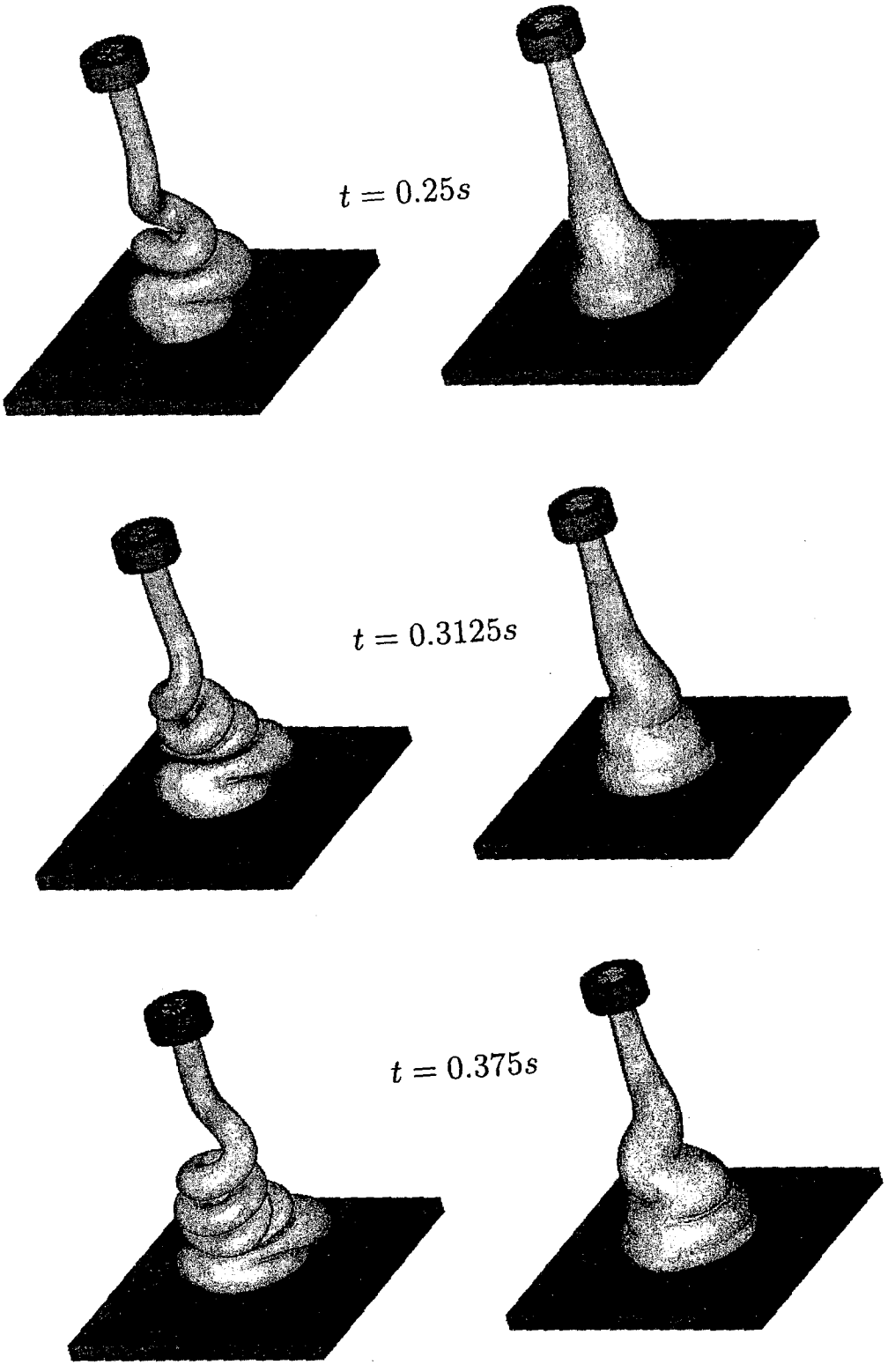

Fig. 18. Continued.

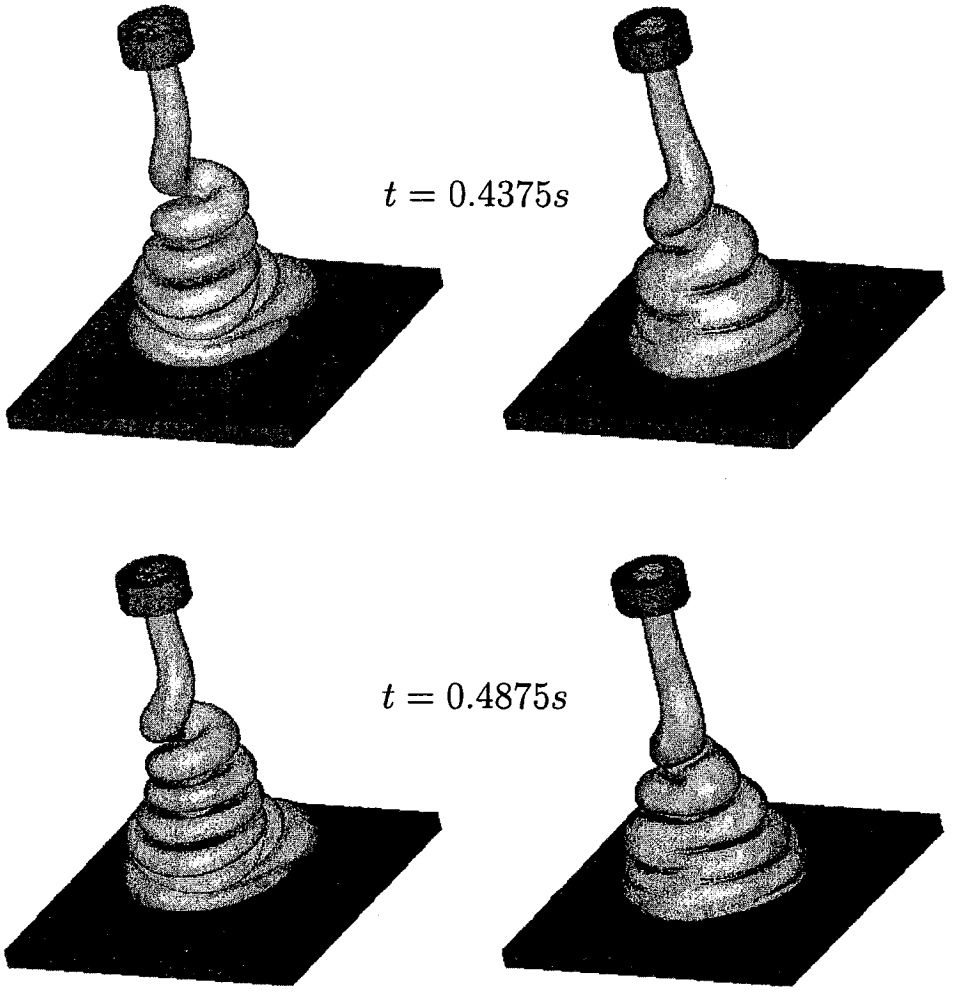

Fig. 18. Continued.

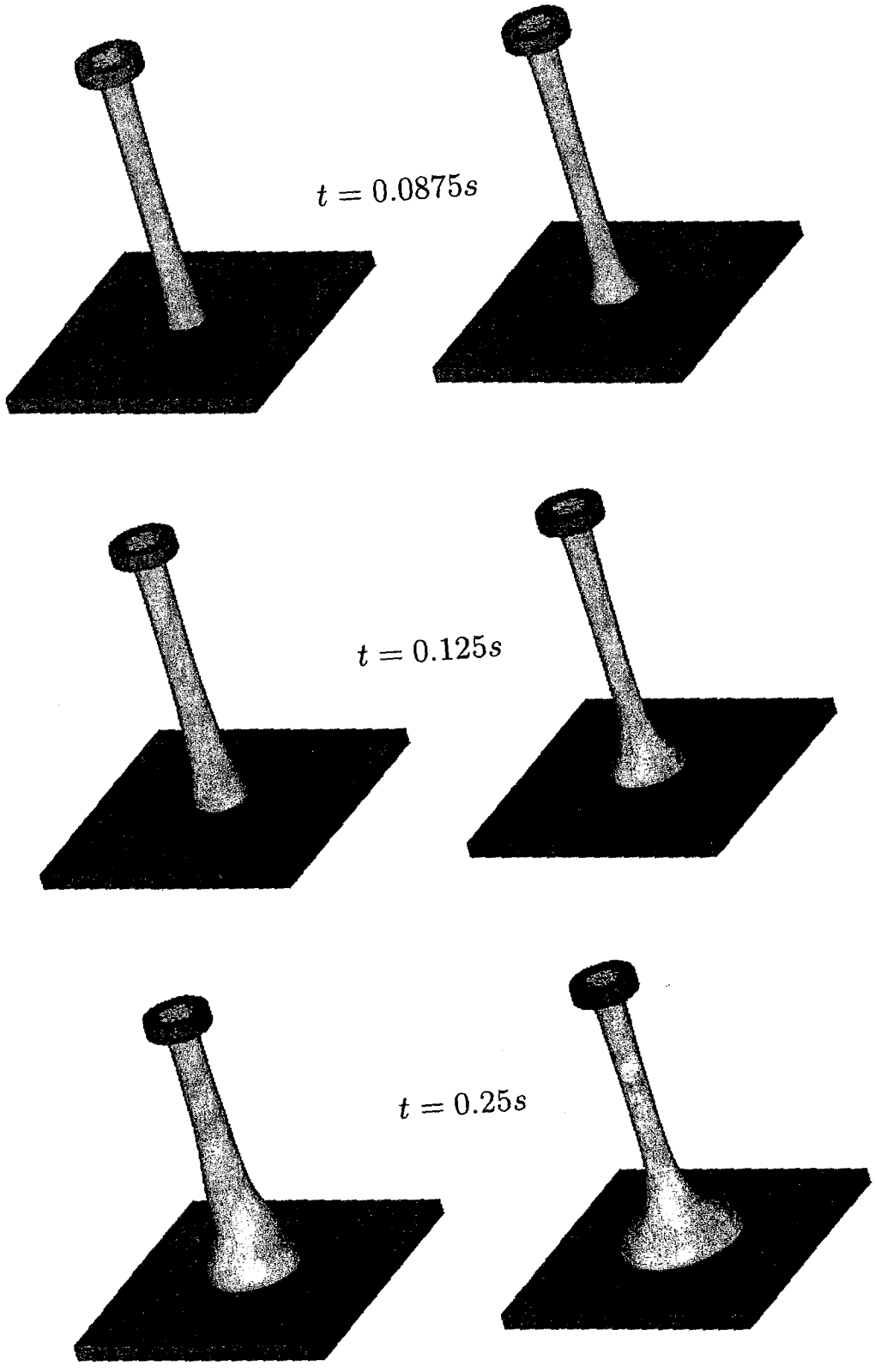

Fig. 19. Numerical simulation of three-dimensional jet buckling. Newtonian jet (on the left) and non-Newtonian jet (on the right). Fluid flow visualization at different times - 3D-view. $Re = 0.60$.

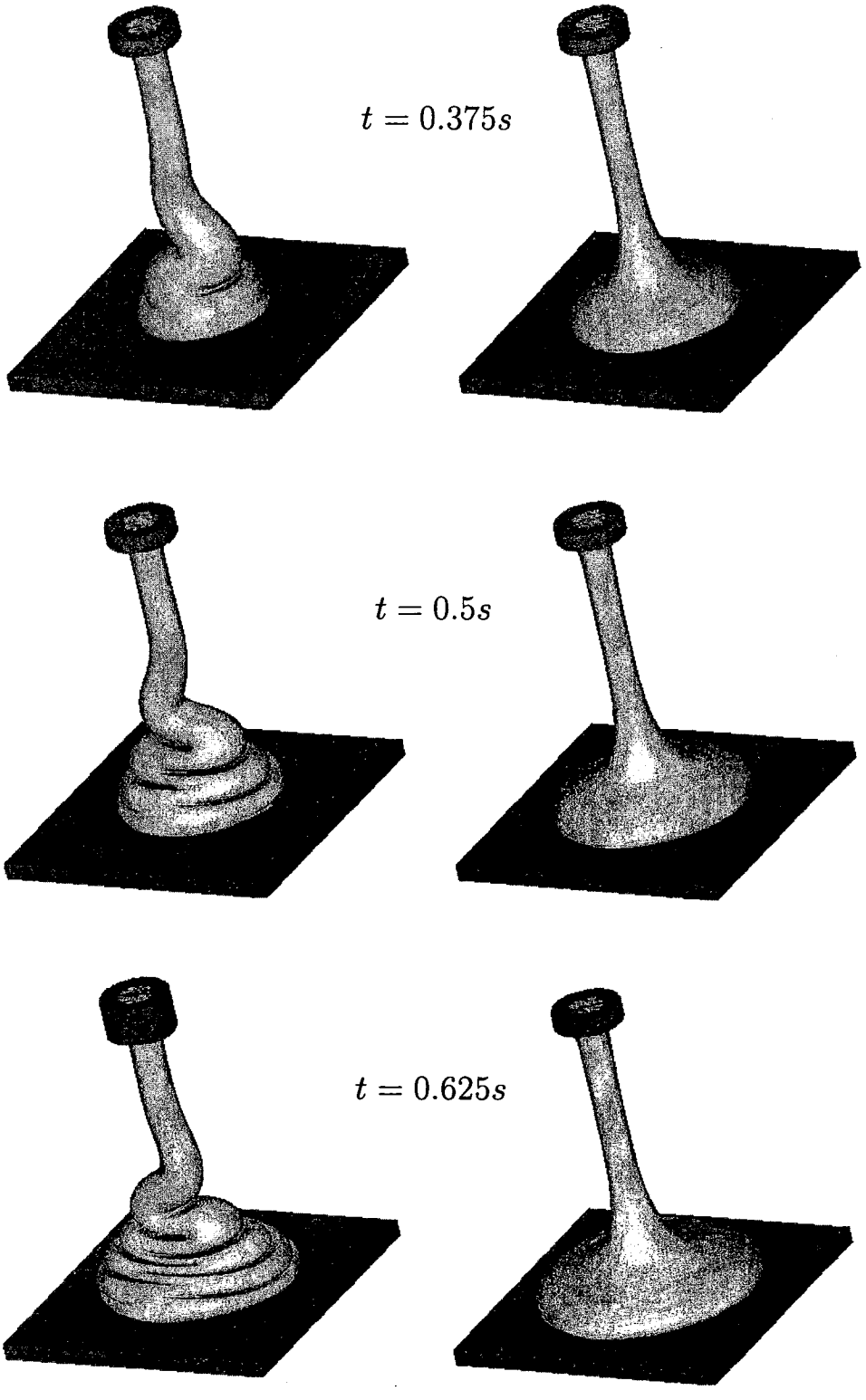

Fig. 19. Continued.

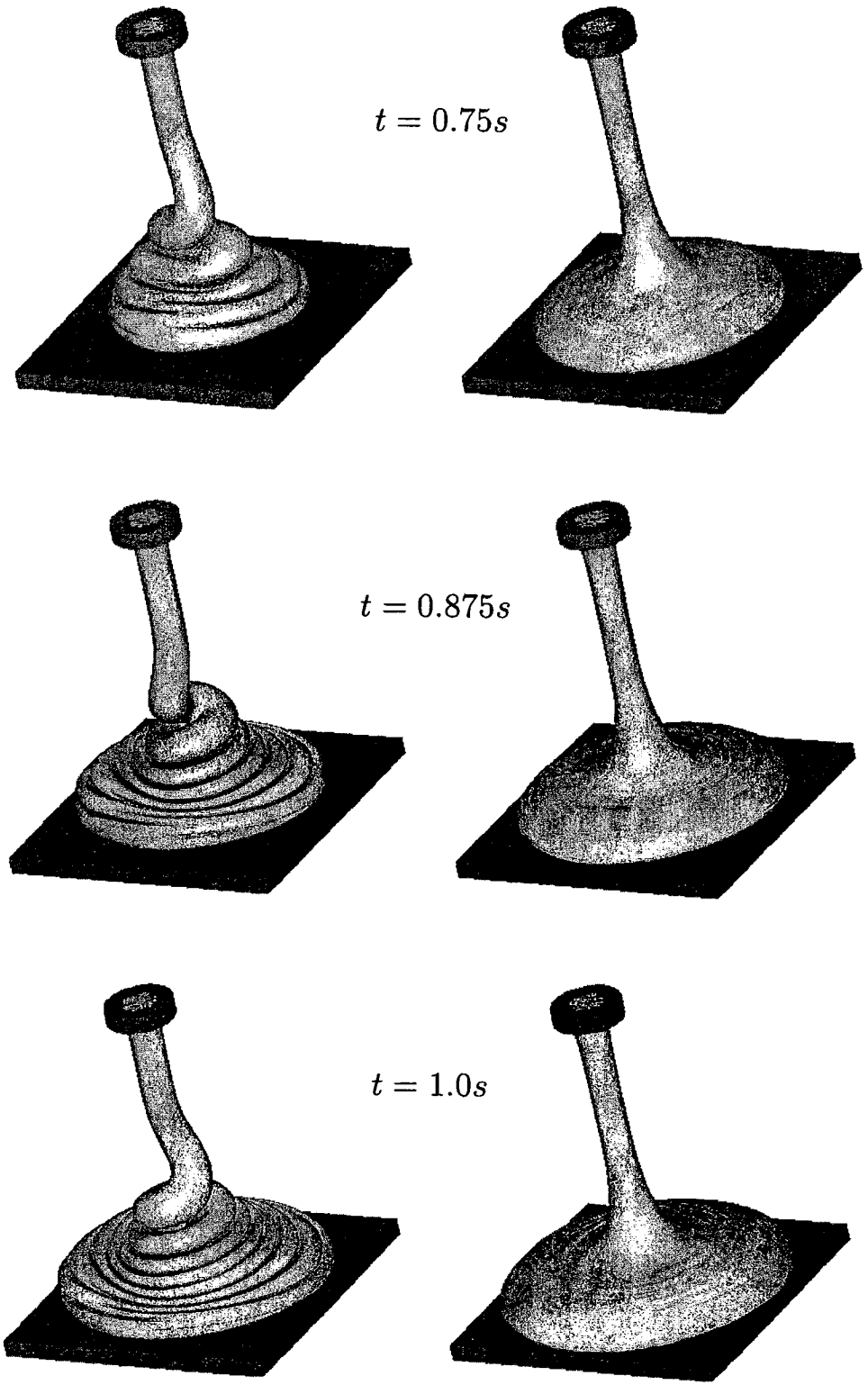

Fig. 19. Continued.

6.3 Numerical Simulation of Drop Spreading

To further demonstrate that the numerical technique presented in this paper can compute free surface flows of a shear-thinning fluid the spreading of a drop was simulated. A flat surface of dimensions 10cm × 10cm and a drop of fluid having a radius $R = 1$cm were considered. The drop was situated 4 cm above the surface with an initial velocity of $U = 1\text{ms}^{-1}$ and the drop was let fall vertically onto the flat surface. Gravity is acting in the negative z-direction with $g = -9.81\ \text{ms}^{-2}$. The fluid was modelled by the Cross model characterised by $\nu_0 = 0.01\text{m}^2\text{s}^{-1}$, $\nu_\infty = 0.0005\text{m}^2\text{s}^{-1}$, $K = 1.0$ and $m = 1.0$. The scaling parameters for this simulation were U, R and ν_0. We ran the FreeFlow–3D code with this input data for both a Newtonian drop with constant viscosity ν_0 and a non-Newtonian drop with the Cross model specified above. The results are displayed in figure 20.

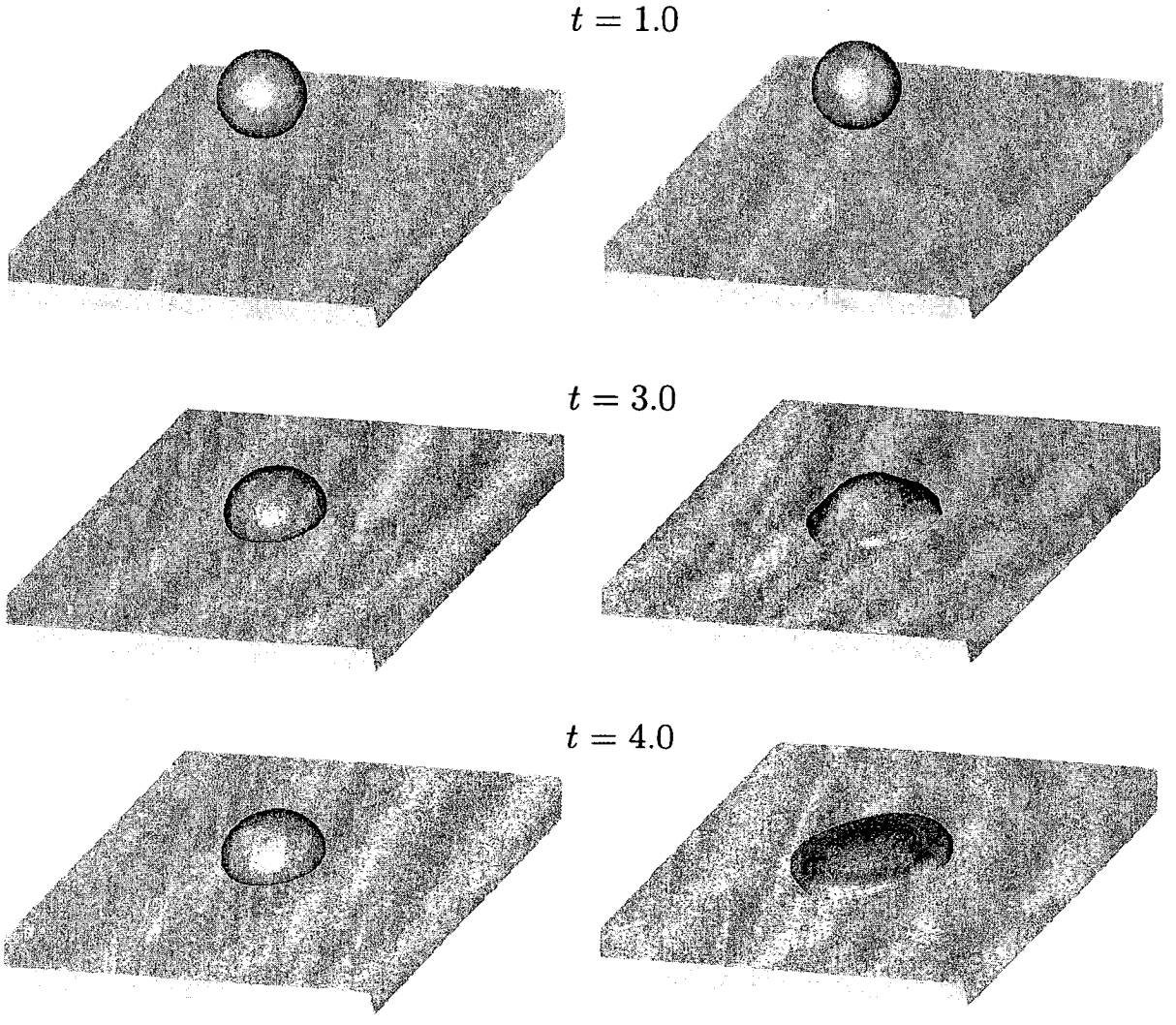

Fig. 20. Numerical simulation of the spreading of a drop. Newtonian drop (on the left) and non-Newtonian drop (on the right). Three-dimensional fluid flow visualization at different times.

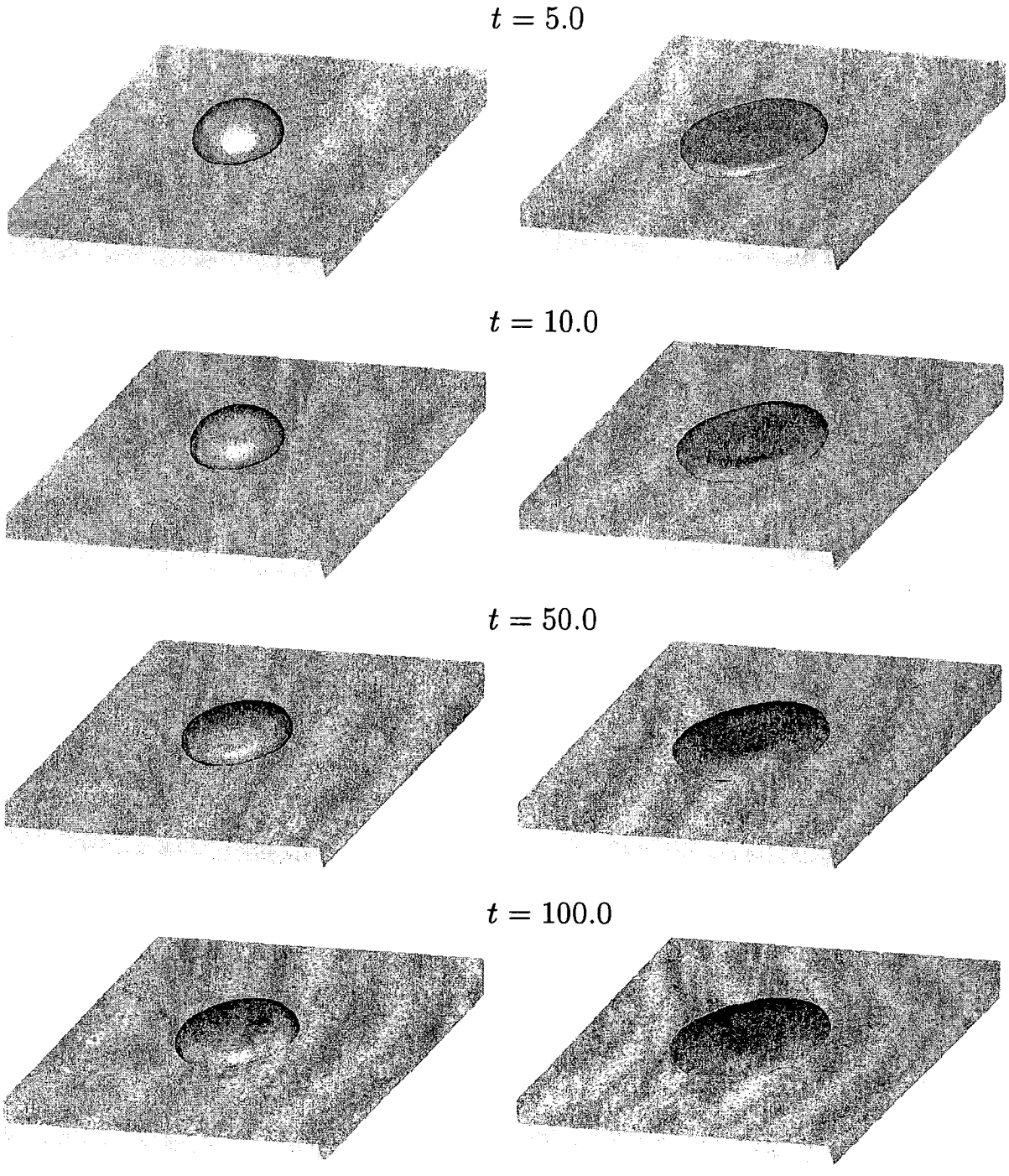

Fig. 20. Continued.

Upon impingement the fluid flow of the two drops is noticeably different and the differences are almost entirely due to thin shearing effects. At time $t = 3$ the generalized Newtonian drop spreads rapidly in a radial direction. By time $t = 4.0$ fluid from the centre catches up producing a distinct rim with an annular indentation. This rim is then accelerated leaving at time $t = 5.0$ a central depression. As the central depression becames less marked so the rim disappears leaving a thin advancing perimeter.

7. Concluding Remarks

This paper presented a finite difference technique for solving three-dimensional generalized Newtonian free surface flows. The numerical method described herein is a considerable extension of the technique presented by Tomé et al. [18] to three dimensions. In this work attention has been given to the implementation of the full 3D-free surface stress conditions. The finite difference equations presented have been implemented to produce a three-dimensional code. Analytic solutions for fully developed flow in a pipe governed by the Cross model have been derived. These analytic solutions were then compared to the numerical results and the agreement between the two solutions was good. It is pointed out that Couette flow can be physically unstable when a function of the shear rate is exceeded. From simulations this appears to have a certain universality and this is demonstrated by a jet impinging on a plate. Several three-dimensional generalized Newtonian free surface flows have been simulated, namely, jet impinging on a flat surface, jet buckling and drop spreading. All these simulations clearly displayed the behaviour of shear-thinnings fluids. In particular, the simulation of jet buckling showed that under certain circumstances a Newtonian jet may buckle while a generalized Newtonian jet may not; this concurs with results obtained by Tomé et al. [18] for the two-dimensional case.

Acknowledgements

We would like to acknowledge financial support of the Brazilian agency FAPESP (Fundação de Amparo a Pesquisa do Estado de São Paulo) Grant no. 00/03385-0.

References

[1] A.A. Amsden and F.H. Harlow, The SMAC method: a numerical technique for calculating incompressible fluid flow, Los Alamos Scientific Laboratory, Report LA-4370 (1970).

[2] A. Castelo, M.F. Tomé, C.N.L. César, J.A. Cuminato, S. McKee, Freeflow: An integrated simulation system for three-dimensional free surface flows, Comput. Visual. Sci., **2**, 199-210 (2000).

[3] H. Court, A.R. Davies and K. Walters, Long-range memory effects in flows involving abrupt changes in geometry, Parti IV. Numerical simulation using integral rheological models, J. Non-Newtonian Fluid Mech., **8**, 95-117 (1981).

[4] M.J. Crochet, A.R. Davies and K. Walters, Numerical Simulation of Non-Newtonian Flow, Elsevier, 1984.

[5] J.O. Cruickshank, Low-Reynolds-number Instabilities in Stagnating Jet Flows, J. Fluid. Mech., **193**, 111–127 (1988).

[6] J.O. Cruickshank and B. R. Munson, Viscous-fluid buckling of plane and axisymmetric jets, J. Fluid. Mech., **113**, 111–127 (1981).

[7] V.G. Ferreira, M.F. Tome, N. Mangiavacchi, A. Castelo, J.A. Cuminato, A.O. Fortuna, S. McKee, High Order Upwinding and the Hydraulic Jump, *Int. J. Numer. Meth. Fluids*, **39**, 549-583 (2002).

[8] I.S. Gradshteyn, I.M. Ryzhik, Table of Integrals, Series and Products, Academic Press, London, 1980.

[9] M. Griebel, T. Dornseifer and T. Neunhoeffer, Numerical Simulation in Fluid Dynamics: a practical introduction. SIAM publications, 1997.

[10] F. Harlow and J.E. Welch, Numerical calculation of time-dependent viscous incompressible flow of fluid with a free surface, Phys. Fluids, **8**, 2182-2189 (1965).

[11] X-L. Luo, Numerical simulation of Weissenberg phenomena - the rod-climbing of viscoelastic fluids, Computer Methods in Applied Mechanics and Engineering, **180**, 393-412 (1999).

[12] M. Mäntylä, *An Introduction to Solid Modeling*, Computer Science Press, Rockville, Md., 1988.

[13] G.J. Manogg, P. Townsend and M.F. Webster, Numerical simulation of multilayer injection moulding, J. Non-Newtonian Fluid Mech., **68**, 153-167 (1997).

[14] M. Renardy, Local existence of solutions of the Dirichlet initial-boundary value problem for incompressible hypoelastic materials, SIAM J. Math. Anal., **21**, 1369-1385 (1990).

[15] T. Sato and S.M. Richardson, Explicit numerical simulation of time-dependent viscoelastic flow problems by a finite element/finite volume method, J. Non-Newtonian Fluid Mech., **51**, 249-275 (1994).

[16] W. Shyy, H. S. Vdaykumar, M. M. Rao and R. W. Smith, Computational Fluid Dynamics with Moving Boundaries (Taylor and Francis, Washington, DC, 1996).

[17] R.I. Tanner and K. Walters, Rheology: An Historical Perspective, Elsevier, 1998.

[18] M.F. Tomé, B. Duffy and S. McKee, A numerical technique for solving unsteady non-Newtonian free surface flows, J. Non-Newtonian Fluid Mech., **62**, 9-34 (1996).

[19] M.F. Tome, A. Castelo F., J.A. Cuminato and S. McKee, GENSMAC3D: Implementation of the Navier-Stokes Equations and Boundary Conditions for 3D Free Surface Flows, Universidade de São Paulo, Departamento de Ciência de Computação e Estatística, *Notas do ICMC no. 29*, (1996).

[20] M.F. Tome, A. Castelo F., J.A. Cuminato, N. Mangiavacchi and S. McKee, GENSMAC3D: a numerical technique for solving three-dimensional free surface flows, Int. J. Numer. Meth. in Fluids, **37**, 747-796 (2001).

[21] M.F. Tomé and S. McKee, GENSMAC: A computational marker-and-cell method for free surface flows in general domains, J. Comput. Phys., **110**, 171-186 (1994).

[22] M.F. Tomé and S. McKee, Numerical Simulation of Viscous Flow: Buckling of Planar Jets, Int. J. Numer. Meth. Fluids, **29**, 705–718 (1999).

[23] M.F. Tomé, N. Mangiavacchi, J.A. Cuminato, A. Castelo, S. McKee, *A Numerical Technique for Solving Unsteady Viscoelastic Free Surface Flows*, Journal of Non-Newtonian Fluid Mech., **106**, 61-106 (2002).

[24] A. Varonos and G. Bergeles, Development and assessment of a variable-order non-oscillatory scheme for convection term discretization, *Int. J. Numer. Meth. Fluids*, **26** (1998), 1-16.

[25] S-C. Xue, N. Phan-Thien and R.I. Tanner, Numerical study of secondary flows of viscoelastic fluid in straight pipes by an implicit finite volume method, J. Non-Newtonian Fluid Mech., **59**, 191-213 (1995).

[26] S-C. Xue, R.I. Tanner, N. Phan-Thien, Three-dimensional Numerical Simulation of Viscoelastic Flow – Predictability and Accuracy, Computer Methods in Applied Mechanics and Engineering, **180**, 305-331 (1999).

NOTAS DO ICMC

SÉRIE COMPUTAÇÃO

070/2003 SANTOS, F.L.P.; MANGIAVACCHI, N.; CASTELO, A.; TOMÉ, M.F.; CUMINATO, J.A. – A novel technique for free surface 2D multiphase flows.

069/2003 VIANNA, A.C.G.; ARENALES, M.N.; GRAMANI, M.C.N. – Two-stage and constrained two-dimensional guillotine cutting problems.

068/2003 ARAUJO, S.A.; ARENALES, M.N.; CLARK, A.R. – A lot-sizing and scheduling problem in a foundry.

067/2003 ARAUJO, S.A.; ARENALES, M.N. – Dimensionamento de lotes e programação do forno numa fundição automatizada de porte médio.

066/2002 VALERIO NETTO, A.; OLIVEIRA, M.C.F. – Industrial application trends and market perspectives for virtual reality and visual simulation.

065/2002 VALERIO NETTO, A.; OLIVEIRA, M.C.F. – Desenvolvimento de um protótipo de um torno CNC utilizando realidade virtual.

064/2002 MARQUES, F.P.; ARENALES, M.N. - O problema da mochila compartimentada e aplicações.

063/2001 TOMÉ, M F; MANGIAVACHI, N; CUMINATO, J A; CASTELO, A – A marker-and-cell technique for simulating unsteady viscoelastic free surface flows.

062/2001 VARGAS, A J C; NONATO, L G. – β-conexão: uma família de objetos tridimensionais reconstruídos a partir de seções planares.

061/2001 OLIVEIRA JR., O N; MARTINS, R T; RINO, L H M ; NUNES, M G V – O uso de interlínguas para comunicação via internet: o projeto UNL/Brasil.